Article

Effect of Zinc Oxide Nano-Additives and Soybean Biodiesel at Varying Loads and Compression Ratios on VCR Diesel Engine Characteristics

Rakhamaji S. Gavhane [1], Ajit M. Kate [2], Abhay Pawar [3], Mohammad Reza Safaei [4,5,6,*], Manzoore Elahi M. Soudagar [7], Muhammad Mujtaba Abbas [7], Hafiz Muhammad Ali [8], Nagaraj R Banapurmath [9], Marjan Goodarzi [10], Irfan Anjum Badruddin [11], Waqar Ahmed [7] and Kiran Shahapurkar [12]

[1] Department of Mechanical Engineering, Amrutvahini College of Engineering, Sangamner, Ahmednagar 422608, India; rakhmaji.gavhane@avcoe.org

[2] Department of Mechanical Engineering, Zeal College of Engineering and Research, Pune 411041, India; ajit.kate@zealeducation.com

[3] Department of Mechanical Engineering, D Y Patil College of Engineering, Ambi Talegaon Tal Maval, Pune 410506, India; abhay.pawar@dyptc.edu

[4] Institute of Research and Development, Duy Tan University, Da Nang 550000, Vietnam

[5] Faculty of Electrical—Electronic Engineering, Duy Tan University, Da Nang 550000, Vietnam

[6] Department of Civil and Environmental Engineering, Florida International University, Miami, FL 33174, USA

[7] Department of Mechanical Engineering, Faculty of Engineering, University of Malaya, Kuala Lumpur 50603, Malaysia; manzoor@siswa.um.edu.my (M.E.M.S.); m.mujtaba@uet.edu.pk (M.M.A.); Hva80013@siswa.um.edu.my (W.A.)

[8] Mechanical Engineering Department, King Fahd University of Petroleum and Minerals (KFUPM), Dharan 31261, Saudi Arabia; hafiz.ali@kfupm.edu.sa

[9] Department of Mechanical Engineering, B.V.B. College of Engineering and Technology, KLE Technological University, Vidyanagar, Hubli 580031, India; nr_banapurmath@kletech.ac.in

[10] Sustainable Management of Natural Resources and Environment Research Group, Faculty of Environment and Labour Safety, Ton Duc Thang University, Ho Chi Minh City 700000, Vietnam; marjan.goodarzi@tdtu.edu.vn

[11] Research Center for Advanced Materials Science (RCAMS), King Khalid University, P.O. Box 9004, Abha 61413, Kingdom of Saudi Arabia; irfan@kku.edu.sa

[12] Department of Mechanical Design and Manufacturing Engineering, School of Mechanical, Chemical and Materials Engineering, Adama Science and Technology University, Adama 1888, Ethiopia; kiranhs1588@astu.edu.et

* Correspondence: mohammadrezasafaei@duytan.edu.vn; Tel.: (+1)-502-657-9981

check for updates

Abstract: The present investigation is directed towards synthesis of zinc oxide (ZnO) nanoparticles and steady blending with soybean biodiesel (SBME25) to improve the fuel properties of SBME25 and enhance the overall characteristics of a variable compression ratio diesel engine. The soybean biodiesel (SBME) was prepared using the transesterification reaction. Numerous characterization tests were carried out to ascertain the shape and size of zinc oxide nanoparticles. The synthesized asymmetric ZnO nanoparticles were dispersed in SBME25 at three dosage levels (25, 50, and 75 ppm) with sodium dodecyl benzene sulphonate (SDBS) surfactant using the ultrasonication process. The quantified physicochemical properties of all the fuels blends were in symmetry with the American society for testing and materials (ASTM) standards. Nanofuel blends demonstrated enhanced fuel properties compared with SBME25. The engine was operated at two different compression ratios (18.5 and 21.5) and a comparison was made, and best fuel blend and compression ratio (CR) were selected. Fuel blend SBME25ZnO50 and compression ratio (CR) of 21.5 illustrated an overall enhancement in engine characteristics. For SBME25ZnO50 and CR 21.5 fuel blend, brake thermal efficiency (BTE) increased by 23.2%, brake specific fuel consumption (BSFC) were reduced by 26.66%, and hydrocarbon (HC),

CO, smoke, and CO_2 emissions were reduced by 32.234%, 28.21% 22.55% and 21.66%, respectively; in addition, the heat release rate (HRR) and mean gas temperature (MGT) improved, and ignition delay (ID) was reduced. In contrast, the NOx emissions increased for all the nanofuel blends due to greater supply of oxygen and increase in the temperature of the combustion chamber. At a CR of 18.5, a similar trend was observed, while the values of engine characteristics were lower compared with CR of 21.5. The properties of nanofuel blend SBME25ZnO50 were in symmetry and comparable to the diesel fuel.

Keywords: soybean biodiesel; zinc oxide nanoparticles; compression ratio; VCR engine performance; emissions

1. Introduction

The global increase in fuel consumption and dependence on petroleum, and the increasing costs due to higher demand, have sparked interest in alternate and sustainable energy sources [1]. Developing nations are highly dependent on fossil fuels, particularly for their industrial and transport sectors [2]. Currently, due to an inadequate supply of fossil fuels, increasing global prices for crude oil and environmental factors have led to renewable energy sources becoming increasingly more important [3,4]. Vegetable oils have certain comparable diesel fuel properties and are known to have several advantages over fossil fuels, such as being environmentally friendly, nontoxic, and biodegradable, and thus help in establishing environmental balance [5,6]. Their cetane number and vaporization pressure is almost equivalent to that of diesel. Biodiesel contains extra oxygen atoms in its molecular structure, which contribute oxygen that assist in enhanced fuel combustion. Nonetheless, despite the numerous advantages of biodiesel, it has certain disadvantages, such as high viscosity, poor cold flow properties and characteristics, and lower heating value [1,7,8]. A recently developed technique to improve combustion characteristics and fuel properties is through the addition of fuel additives. The past decade has witnessed a rise in the utilization of alcohol-based additives in biodiesel fuel blends, such as ethanol, butanol, heptanol, and diethyl ether [9–11]. Alcohol-based additives supply more oxygen in the combustion chamber to reduce emissions, however, due to the formation of a lean mixture it lowers the calorific value, which, combined with higher auto ignition temperatures and lower lubrication properties, results in engine deterioration and reduced performance characteristics. Hence, researchers have explored the potential of micro- and nanoparticle additives. Microparticle additives assisted in improving the engine characteristics, but they tend to agglomerate. Nanotechnology has found a suitable place in many industrial applications, such as engineering, agricultural and medical science, biotechnology, and transport. Nanoparticle additives exhibit higher thermophysical properties and ease of miscibility in any base fluids [12–16]. Previous investigators reported nanoparticle additives to be exceptionally effective in reducing the agglomeration in comparison with microparticles and improve engine characteristics due to the large surface air-to-volume ratio, high thermophysical properties, high combustion velocity, and high thermal conductivity [17–19]. In addition, the addition of nanoparticles to base fluids improves the physiochemical properties, in the form of higher flash point, fire point, cloud point, and calorific value, and lower density and viscosity of the base fluid [1,7,14,20–23]. Table 1 shows the effect of nanoparticles in different fuel blends. Recent studies on the effect of nanoparticles and biodiesel in diesel engines reported an enhancement in combustion characteristics, such as cylinder pressure, heat release rate (HRR), and mean gas temperature (MGT), and reduced the ignition delay (ID) period for metal and carbon-based nano-additives, such as carbon nanotubes, graphene oxide, Cu_2O, $FeCl_3$, CeO_2, Co_3O_4, Al_2O_3, TiO_2, and ZnO.

Table 1. The effect of nanoparticles in different fuel blends.

Biofuel Blends	Biodiesel	Dosage of NPs	Engine Type	Application Output	Ref.
D (80%) + BD (20%)	Dairy scum oil methyl ester	Graphene oxide 20 ppm 40 ppm 60 ppm	SC, DI, 4-S, CI engine, 23°BDTC, WC, 17.5 CR, 3 FI nozzles	• Dosage level of 40 ppm of GNPs increased the BTE, HRR and reduced the BSFC, ignition delay. • The calorific value increased while the viscosity reduced. • The emissions, CO, HC and smoke reduced. • The NOx emission slightly increased.	[7]
D (80%) + BD (20%)	Pongamia oil methyl ester	FeO 30 nm and Ferrofluid 100 nm	SC, DI, 4-S, CI engine, 23°BTDC, WC, 17.5 CR, 3 FI nozzles	• Improves the peak HRR, BTE. • Reduction in NOx emissions. • BSFC reduces for Nanofuel blends. • Reduction in CO, HC, PM, smoke.	[24]
D (40%) + BD (30%) + ethanol (30%)	Palm oil methyl ester	ZnO 250 ppm	SC, DI, 4-S, CI engine, 23°BTDC, WC, 17.5 CR, 3 FI nozzles	• Reduction of BSFC, HRR and cylinder pressure. • Decrease in CO, NOx, smoke and BTE. • Increases the calorific value.	[25]
D (70%) + BD (20%) + ethanol (10%)	Castor oil methyl ester	γ-Alumina 10 ppm 20 ppm 30 ppm	SC, DI, 4-S, CI Engine, 23°BTDC HCC, AC, 17.5 CR 3 FI nozzles, 0.3 mm dia. FI holes, 661 cc	• Improved BTE, Cylinder pressure and heat release rate. • Lower HC, CO emissions, BSEC.	[26]
BD (91%) + 50 mL DEE	Jatropha methyl ester	CNT 50 ppm	SC, DI, 4-S, CI Engine, 26°BTDC HCC, AC, 17.5 CR 3 FI nozzles	• The CO, HC and NOx reduced in comparison with neat diesel. • Enhanced combustion attributes, micro explosion of fuel droplets. • Improved BTE and reduced BSFC.	[27]
D (70%) + BD (10%) + ethanol (20%) (Diesterol- E20)	Castor oil methyl ester	Ceria and CNT 25 ppm 50 ppm 100 ppm	CI, WC, DI, 1500 rpm, 19:1, 23°BTDC	• Accelerates the burning rate, lowers the ID and HRR. • Improves the peak HRR, BTE. • Reduces the NOx, smoke and HC. • Avoids the accumulation of non-polar complexes on the cylinder wall.	[28]
BD + (200 and 500 ppm of Ethanox)	Calophyllum Inophyllum Methyl Ester	ZnO 50 ppm 100 ppm	2-C, DI, 4-S, CI Engine, 23°BTDC, WC, 18.5 CR, 5 FI nozzles, 1670 cc	• Catalytic effect of NPs and micro explosion improved BTE, HRR and cylinder gas pressure. • Better atomization and rapid evaporation. • NOx was reduced. • Supply of excess O leads in lower CO and HC.	[29]
D (70%) + BD (20%) + ethanol (10%)	Jatropha methyl ester	γ-Alumina 10 ppm 20 ppm 30 ppm	SC, DI, 4-S, CI Engine, 23°BTDC HCC, AC, 17.5 CR, 3 FI nozzles, 0.3 mm dia. FI holes, 661 cc	• Improved BTE, Cylinder pressure and heat release rate. • Lower HC, CO emissions, BSEC. • Lower NOx emissions.	[30]

D: Diesel; BD: Biodiesel; WC: Water Cooled; SC: Single Cylinder; AC: Air Cooled; 4-S: Four Stroke; DI: Direct Injection; CI: Compression-Ignition; FI: Fuel Injector; CR: Compression ratio; BTDC: Before Top Dead Center.

Özgür et al. [31] investigated the combined effect of the addition of 25 and 50 mg/L of MgO and SiO$_2$ nanoparticles in diesel. The authors observed that the addition of nanoparticles in diesel fuel lowered the NOx and CO, and increased the engine performance marginally. Soudagar et al. [7,32] studied the influence of graphene oxide and Al$_2$O$_3$ nanoparticles (20, 40, and 60 ppm) in dairy scum methyl ester and honge oil methyl ester. Sodium dodecyl sulfate surfactant was used for nanoparticle stabilization of nanofuel in the base fluid and the ultrasonication process was carried out for proper blending of fuel blends. The authors reported an enhancement in the overall combustion and performance characteristics, and reduction in hydrocarbon (HC), CO, and smoke opacity, of a conventional mechanical fuel injection system diesel engine for the all the nanofuel blends in contrast to B20 fuel. Karthikeyan et al. [33] performed a related study introducing ZnO nanoparticles to canola biodiesel. They observed that for the B20+ZnO fuel blends, the brake thermal efficiency (BTE) increased, and HC and CO decreased, in comparison with neat B20. The influence of alumina (Al$_2$O$_3$) nanoparticles on biodiesel blends was investigated by Venu and Madhavan [34]. The authors reported the Al$_2$O$_3$ in biodiesel reduced the brake specific fuel consumption (BSFC), NO$_X$, HC, and carbon dioxide despite the increased emission of CO. Sajith et al. [35] studied the influence of CeO$_2$ nanoparticles in biodiesel fuel blends. In order to achieve optimum efficiency, different dosing levels of CeO$_2$ nanoparticles (20, 40, 60, and 80 ppm) were used. The impact of CeO$_2$ nanoparticles on compression-ignition (CI) engine efficiency, thermophysical properties of the fuel, and emissions characteristics were investigated. The authors reported a decline in the NOx and HC emissions and enhancement in the overall engine characteristics. Keskin et al. [36] reported the influence of nanoparticles on specific fuel consumption (SFC) and emission characteristics of diesel engines. The MnO$_2$ and MgO nanoparticles were added to the diesel at concentration levels of 8 and 16 µmol/L. The physiochemical properties of diesel fuel were enhanced due to addition of the nanoparticles. The addition of combined nano-additives reduced CO by 16%, smoke opacity by 29%, and the SFC by 4.16%, whereas a 10% increase in NOx emissions was recorded. Consequently, the previous literature suggests that the addition of nanoparticle additives to biodiesel fuel enhances the overall diesel engine characteristics and the fuel properties. Studies have been carried out using fixed engine variables by numerous investigators.

Regarding environmental pollution due to the addition of nanoparticles in fuel, limited research is available concerning the traces of nano-additives in engine exhaust emissions. Deqing Mei et al. [37] reported CeO$_2$ in diesel fuel enhances the combustion process, while a high dosing level of nano-CeO$_2$ can cause early ignition, which can lead to escaping of nanoparticles through the exhaust. However, the authors found only a trace of nanoparticles and an insignificant effect on particulate matter (PM) emission. Qibai et al. [38] investigated the effects of Al and carbon nanoparticles in a diesel-biodiesel blend; the exhaust gases were passed through diesel particulate filters (DPFs), and slight traces of aluminum, oxygen, carbon, and silicon were found. Toxic effects of nanoparticles on animals include crossing cell membranes and inhaled NPs can reach the blood and target sites such as the heart, blood cells, and liver [1]. The information on these pathways is limited, but the actual number of particles that move from one organ to another can be significant, depending on exposure time [39]. Studies on the environmental pollution caused by nanoparticles as fuel additives are limited, hence there is a scope for further study.

The objective of the current research is to investigate the combined effect of nanoparticle additives and biodiesel fuel blends at varying compression ratios and loads in a variable compression ratio (VCR) diesel engine. The study delves into the potential of a ZnO nanoparticle and soybean biodiesel blend. The soybean biodiesel (SBME25) is blended with synthesized zinc oxide nanoparticles at varying blending ratios of 25, 50, and 75 ppm. This study facilitates and proposes a direction for future research and commercialization of all aspects of nanotechnology in biodiesel fuels in diesel engine applications. In addition, this study enables the selection of optimal and most suitable compression ratios for enhancement of diesel engine characteristics.

2. Material and Methods

2.1. Production of Soybean Biodiesel

A Gas Chromatography Mass Spectrometer (GCMS/MS) Shimadzu, Japan (TQ 8030) was used to analyze the free fatty acid (FFA) percentage in the soybean oil. Table 2 shows the FFA composition of soybean biodiesel.

Table 2. Fatty acid composition of soybean oil.

Fatty Acid	Carbon Chain	Composition (wt.%)
Palmitic	C 16:0	11.24
Stearic	C 18:0	4.15
Oleic	C 18:1	23.69
Linoleic	C 18:2	51.66
Linolenic	C 18:3	6.89

The preparation of biodiesel was carried out at Apex innovations laboratory, India. In the esterification method, the soybean oil was heated with sulfuric acid at 70 °C and methanol in an air-oven for about 60 min to eliminate the moisture. In the subsequent step, i.e., the transesterification reaction, the solution was mixed with sodium hydroxide at 6:1 M and heated at 60 °C for about 60 min. The mixing and heating processes were carried out on a magnetic stirrer rotating at a constant speed of 500 rpm. Then, the solution was transferred to a separating funnel and kept steady for 24 h. After 24 h, a clear distinct layer was visible, distinguishing the glycerol and biodiesel. The lower layer containing glycerol was drained and the upper layer was extracted and washed using warm water. The liquid was dried to obtain soybean biodiesel.
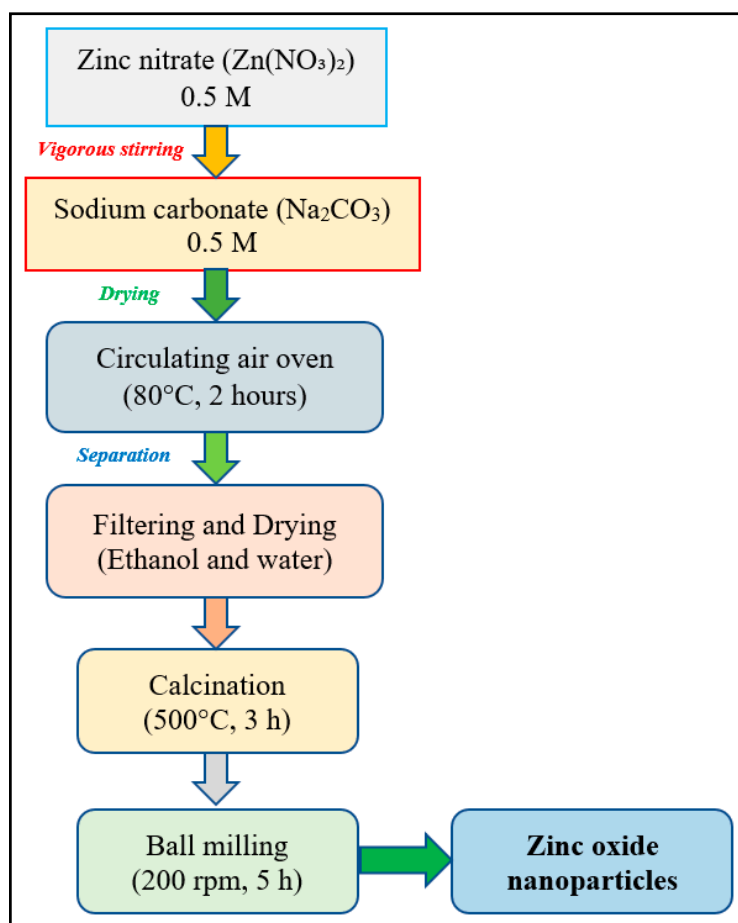
2.2. Synthesis and Characterization of Zinc Oxide Nanoparticles

The zinc oxide nanoparticles were synthesized using the aqueous precipitation method as previously reported Haniffa et al. [40] and Li Yuan et al. [41]. Initially, 0.5 M zinc nitrate ($Zn(NO_3)_2$) was added of drop by drop to 0.5 M of sodium carbonate (Na_2CO_3) solution under vigorous stirring. Soon after separation from the solution using vacuum filtration technique by washing and rinsing three times with distilled water and then ethanol, the precipitate was dried in an air circulating oven at 80 °C for 2 h. The oven-dried powder was calcined to 500 °C for 3 h to obtain zinc oxide nanopowder. Finally, for a period of 5 h the nano powder was ball-milled at 200 rpm to obtain fine zinc oxide nanoparticles. Figure 1 illustrates a flow chart showing the synthesis of zinc oxide nanoparticles using the aqueous precipitation method.

Field emission scanning electron microscope (FESEM) analysis was used to determine chemical composition and visualize the surface morphology of ZnO nanoparticles. The analysis was performed using a Bruker XFlash 6I30, USA. Figure 2 represents the SEM image of ZnO nanoparticles at 25,000× magnification. The synthesized ZnO nanoparticles had Rosette and irregular crystal structures with a wurtzite hexagonal phase, in agreement with previous literature [42,43].

X-ray powder diffraction (XRD) was used to evaluate the crystallinity (phase identification) by comparison with the integrated intensity of a previously reported pattern to that of the observed sharp peaks of the synthesized zinc oxide nanoparticles. The XRD analysis is shown in Figure 3a; the analysis was carried out using a Bruker D8 VENTURE, USA. The calculated hkl values for the peaks observed for ZnO nanoparticles at 2θ = 32.45° (100), 34.64° (002), 36.57° (101), 48.52° (102), 56.43° (110), 62.66° (103), 66.36° (200), 68.13° (112), 69.44° (201), 72.32° (004), and 77.73° (004). A sharp peak was observed at 36.57° (101), which indicates the crystallinity of ZnO nanoparticles; the peaks reported in the current investigation were closer to the characteristic peaks reported by [44,45]. Figure 3b shows the UV-Vis absorption spectra; ultra-violet absorption for ZnO nanoparticles confirms absorbance at a wavelength of 365.47 nm, between the characteristic range of 350 to 380 nm [44].
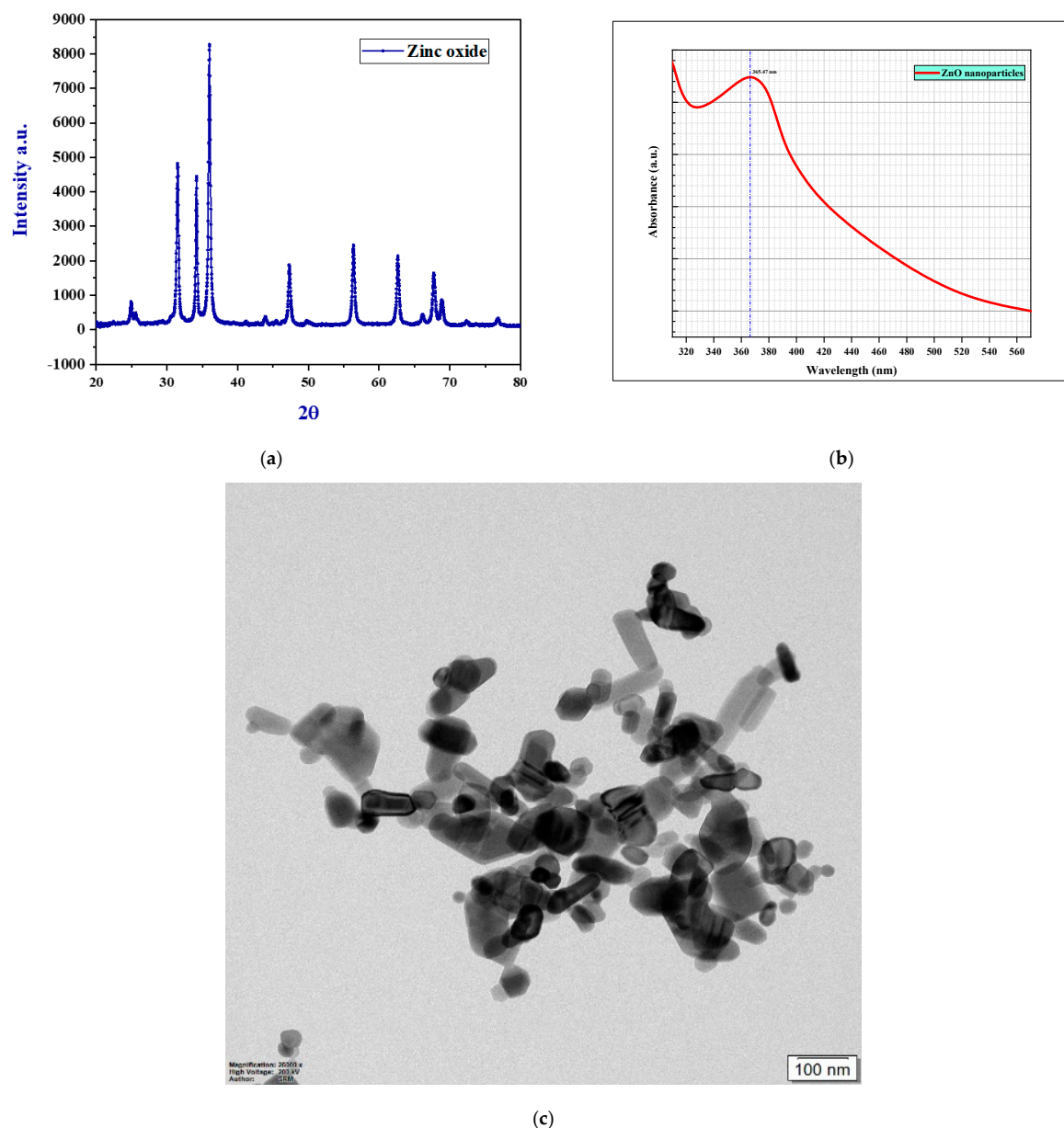
Figure 1. A flow chart of the synthesis of zinc oxide nanoparticles through the aqueous precipitation method.
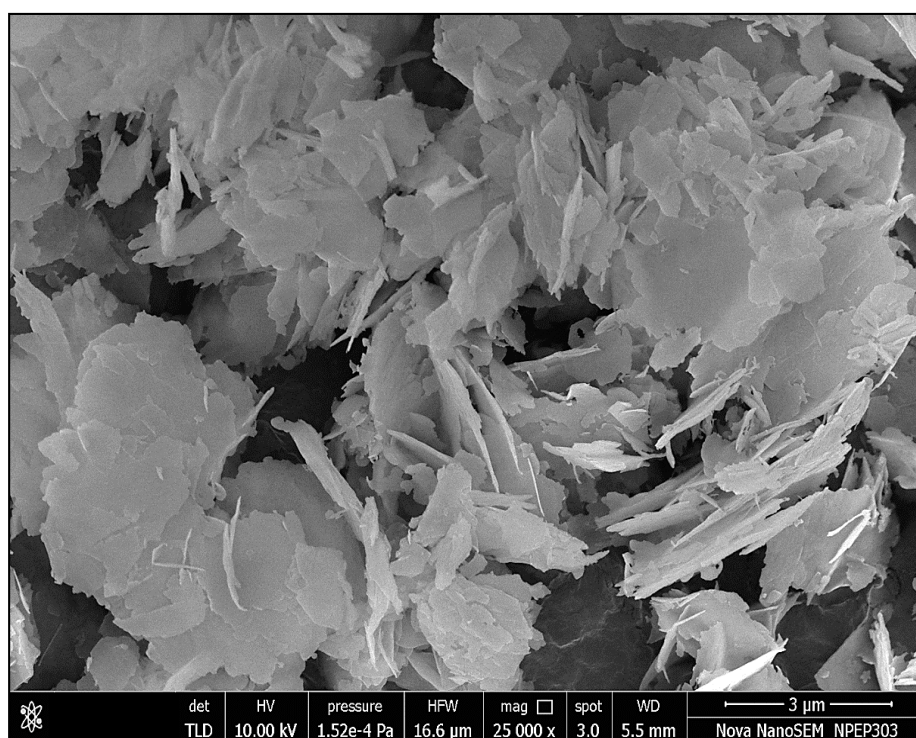
**Figure 2.** FESEM at 3 μm at 25,000× magnification level.

(a)

(b)

(c)

Figure 3. Characterization tests: (**a**) XRD analysis; (**b**) UV-Vis Absorbance; (**c**) TEM at 100 nm magnification.

The main objective of transmission electron microscopy (TEM) analysis is to produce high magnification images of the internal structure of a sample. Figure 3c illustrates the TEM image at 100 nm and magnification level of 20,000×. The TEM analysis is also used to collect data on crystalline structures, contamination, stress, and internal fractures inside materials [44]. Initially, the ZnO nanoparticles were dispersed in ethanol. The structure of ZnO nanoparticles was found to be hexagonal wurtzite and the size of the nanoparticles was in the range of 15–40 nm.

2.3. Preparation and Physiochemical Properties of Nanofuel Blends

A scale was used to measure precise quantities of zinc oxide nanoparticles. The ZnO nanoparticles (25, 50, and 75 mg/L) were mixed with 10 mL of distilled water. Sodium dodecyl sulfate (SDS) surfactant was added for surface modifications and stabilization, to reduce the possibility of coagulation and coalescence, and to reduce the surface tension. Surfactants tend to position themselves at the interface between the nanoparticles and the base fluid, where it establishes a degree of continuity between the

nanoparticles and fluids. The ultrasonication process was carried out for steady blending; initially the ultrasonication bath was used to blend the solution with an agitation time of 60 min. Later, the different nanofluid blends were blended using an ultrasonication probe at a frequency of 15–30 Hz for 20 min. After the zinc oxide nanofluids were prepared they were transferred to the SBME25-diesel fuel blend, and heated and steadily mixed using a magnetic stirrer at 60 °C for 30 min to remove traces of water molecules. Then, the same ultrasonication processes were carried out for a steady dispersion of zinc oxide nanoparticles in SBME25 biodiesel–diesel fuel blend. Figure 4 illustrates the comprehensive steps involved in the preparation of nanofuel.
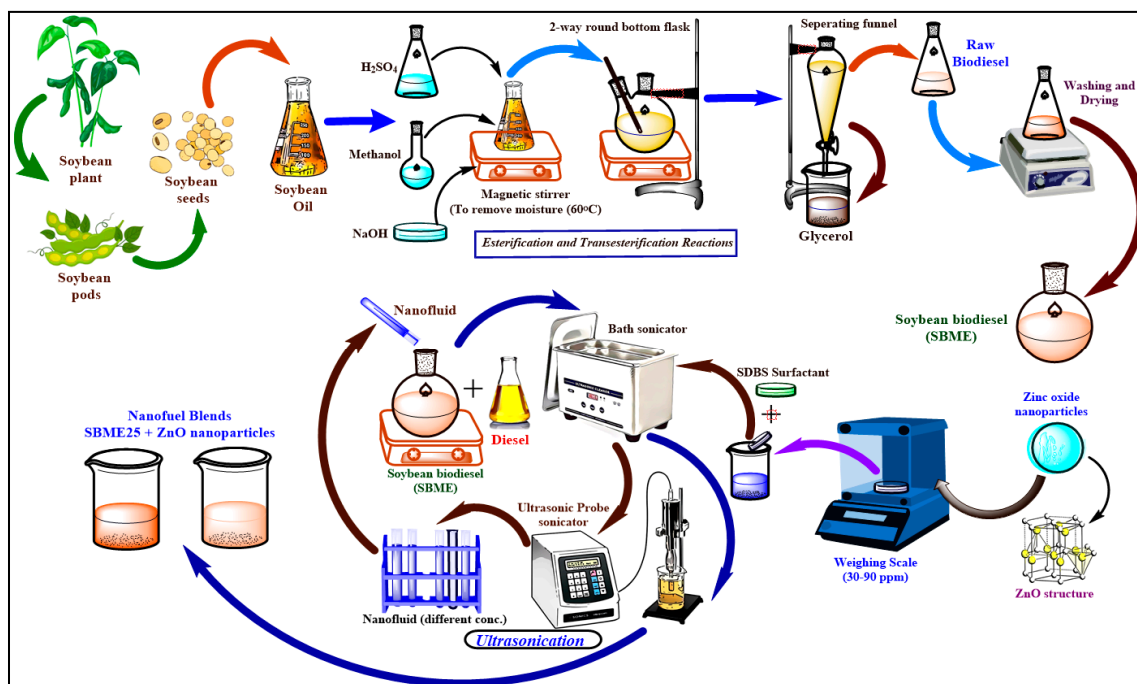
Figure 4. The comprehensive steps involved in the preparation of nanofuel.

The experiments were conducted in various lab facilities available in Maharashtra and Karnataka, India. The detailed description of the equipment, procedure, and lab setup was presented in previous articles by Soudagar et al. [7,32] on the addition of graphene oxide and Al_2O_3 nanoparticles in dairy scum oil methyl ester and honge oil methyl ester. The physiochemical properties of the test fuel blends are demonstrated in Table 3. The analysis indicates the addition of zinc oxide nanoparticles to soybean biodiesel increases the calorific value and cetane number and demonstrates comparable diesel fuel properties. The fuel blend SBME25ZnO50 demonstrated overall improvement in the physicochemical properties. The analyzed results were within the ASTM D6751 standard for biodiesel.

Table 3. Physicochemical properties of fuel blends.

Properties	Unit	ASTM Standards	Test Limit ASTM D6751	Diesel	SBME25	SBME25ZnO25	SBME25ZnO50	SBME25ZnO75
Density	kg/m^3 at 15 °C	D4052	860–900	810	845.66	845.87	846.22	846.84
Calorific value	kJ/kg	D5865	Min. 35,000	45,000	41,684	43,400	44,800	43,850
Kinematic Viscosity	cSt at 40 °C	D445	1.9–6	2.12	3.56	3.52	3.525	3.531
Specific Gravity	gm/cc	D891	0.87–0.90	0.811	0.825	0.820	0.821	0.824
Cetane Number	-	D613	Min. 40	51	48.66	52.55	53.74	53.15
Flash Point	°C	D93	>130	55	65.71	62.87	60.47	61.87
Pour Point	°C	D97-12	−15 to 16	−4	−6	−5	−5.65	−5.6
Cloud Point	°C	D2500-11	−3 to 12	−2	4.5	3.5	3.54	3.57
Sulphur content	% w/w	D5453	0.05	0.005	0.012	0.0156	0.0162	0.0188
Water content	% vol	D2709	0.05% vol	-	Trace	Trace	Trace	Trace

2.4. Uncertainty Analysis of Expected Errors

Uncertainty analysis is an organized set of procedures followed for calculation of errors in experimental data. The inaccuracies occur due to the error in electronic and mechanical components, environmental factors, and human miscalculations. The data is gathered in ideal conditions, and specifications and details of all the components are available. Measurement errors from several different sources are classified into bias and precision errors; throughout the experimentation the bias errors remain constant. In this work, the estimation of experimental uncertainty and the evaluation of standard errors in the measurements were derived using the method proposed by Moffat et al. [46]. Table 4 illustrates the uncertainty and accuracy levels of calculated engine parameters.

Table 4. Uncertainty and accuracy levels of calculated engine parameters.

Parameters	Accuracy (±)	Uncertainty (%)
Brake power (KW)	-	±0.22
Brake thermal efficiency (%)	-	±0.28
Brake specific fuel consumption (%)	-	±0.31
Heat release rate (J/°CA)	-	±0.24
Carbon monoxide emission (%)	±0.01%	±0.18
Nitrogen oxide emission (ppm)	±10 ppm	±0.24
Hydrocarbon emission (ppm)	±10 ppm	±0.14
Exhaust gas temperature (°C)	±1	±0.15
Mean gas temperature (°C)	-	±0.35
Smoke meter (HSU)	±1	±0.25

In addition, the propagation of errors was studied using standard deviations by plotting error bars, where error bars were derived considering the average of six readings. The propagation of uncertainty for various factors are determined depending on two or more independent parameters is carried out using Equation (1):

$$\frac{U_y}{y} = \sqrt{\left(\frac{u_{x_1}}{x_1}\right)^2 + \left(\frac{u_{x_2}}{x_2}\right)^2 + \ldots\ldots\ldots\ldots + \left(\frac{u_{x_n}}{x_n}\right)^n} \tag{1}$$

where U_y: uncertainty; y: testing value; $x_1, x_2,..., x_n$: evaluated parameter; and the uncertainty of emissions is $U_y = \frac{Resolution}{Range}$.

The overall uncertainty of the engine characteristics is calculated using Equation (2):

$$\text{Overall uncertainty} = \pm \sqrt{ \begin{array}{c} Uncertainty~\%~of~(BTE^2 + BSFC^2 + CO^2 + NOx^2 + HC^2 \\ + smoke^2 + HRR^2 + MGT^2 + EGT^2 \end{array}}) = \pm~1.82 \tag{2}$$
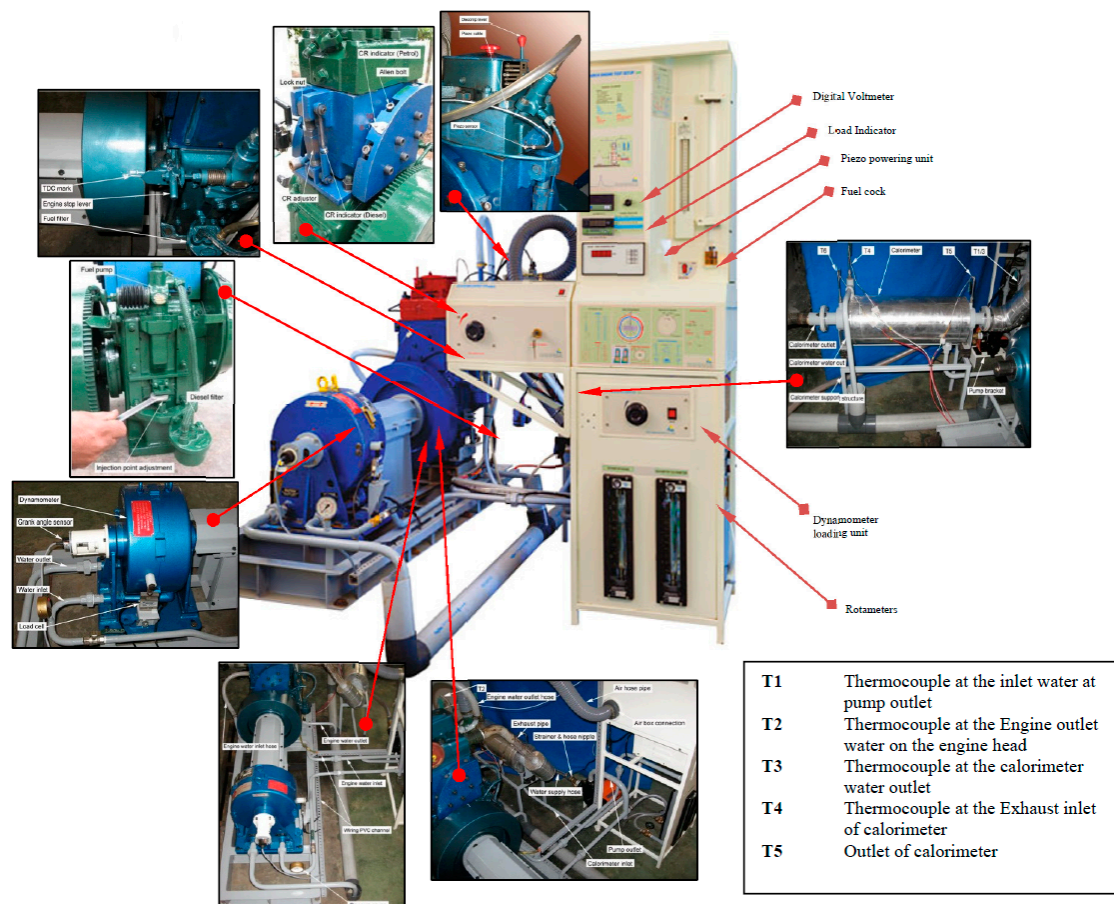
2.5. Test Engine Setup

The engine used in the current investigation is a variable compression ratio (VCR), Kirloskar make, single cylinder diesel engine. All the experiments were carried-out at Apex innovation laboratory, India. The engine was coupled to a five-gas analyzer and smoke meter. The combustion chamber used in the current investigation was hemispherical; compression ratios were varied without stopping the VCR engine and the readings were derived using enginesoft software. A Data Acquisition System (DAQ) and Labview software was used as an interface between the computer and the engine sensors (air and fuel flow, temperatures, and load measurement sensors). Table 5 illustrates the specification of the VCR test engine used in the current investigation.

Figure 5 illustrates the pictorial view of the test engine used in the current investigation. The heat release rate was estimated using the data for 600 crank angle values. The compression ratio was varied by the tilting block arrangement, in which the compression ratio could be varied without stopping the engine. The arrangement consisted of compression ratio indicator and compression ratio adjuster

with a lock nut and six Allen bolts. For varying the compression ratio, the Allen bolts were slightly loosened, and the adjuster lock nut was loosened. Further, the adjuster was rotated to set a desired compression ratio according to the compression ratio indicator, and then locked using a lock nut. The chosen compression ratios in the current investigation were 18.5 and 21.5.

Table 5. Test Engine Specifications.

Number of Strokes	4
Fuel type	Diesel, Biodiesel, and Nanofuel
Cylinder	Single, Water cooled
Rated Power	3.5 KW
Speed	1500 rpm
Cylinder diameter	87.5 mm
Load indicator	Digital, Range 0–50 Kg, Supply 230 V air cooled
Fuel tank	Volume 15 liters with glass fuel metering column
Exhaust Gas Recirculation	Water cooled, Stainless Steel, Range 0–15%
Piezo sensor	Range 5000 PSI, with low noise cable
Temperature sensor	RTD, PT100 and Thermocouple, Type K
Load sensor	Load cell, type strain gauge, range 0–50 Kg
Rotameter	Engine cooling 40–400 LPH; Cal. 25–250 LPH
Dynamometer	
Model	AG10
Make	Saj test plant rig
End flanges both sides	Cardon shaft model 1260 type
Air gap	0.77 mm
Torque	11.5 Nm
Hot coil voltage	60 V
Continuous current (amp)	5
Cold resistance ohm	9.8

T1	Thermocouple at the inlet water at pump outlet
T2	Thermocouple at the Engine outlet water on the engine head
T3	Thermocouple at the calorimeter water outlet
T4	Thermocouple at the Exhaust inlet of calorimeter
T5	Outlet of calorimeter

Figure 5. Variable compression ratio (VCR) test engine setup.

3. Results and Discussions

In this section, the combustion, performance, and emission characteristics of the diesel engine are investigated. The effect of nanofuel blends and compression ratios of 18.5 and 21.5 on heat release rate, ignition delay, BTE, BSFC, and mean gas temperature, and CO, NOx, HC, CO_2, and smoke emissions are reported. A constant speed of 1500 rpm, injection timing (IT) of 23.5°BTDC (before top dead center), and five loads were maintained. Table 6 illustrates the factors considered and employed in the current investigation.

Table 6. Engine parameters.

Factors Considered	Parameters Employed
Engine	Variable Compression Ratio (VCR)
Combustion Chamber (CC)	Hemispherical (HCC)
Injection Pressure (IP)	220 bar
Fuel Injector (FI) holes	4 holes, 0.25 mm dia.
Injection timing (IT)	23°BTDC
Speed	1500 rpm (constant)
Compression Ratio (CR)	18.5, 21.5
Fuel	Diesel, SBME25, SBME25ZnO25, SBME25ZnO50, SBME25ZnO75

*3.1. The Effect of Zinc Oxide Nano Additives and Soybean Fuel Blend on the Engine Performance*

3.1.1. The Effect of SBME25-ZnO Nanofuel Blends on Brake Thermal Efficiency (BTE) at Different Compression Ratios

Figure 6 illustrates the variation of BTE at varying loads. The results demonstrate that the BTE of the VCR diesel engine was enhanced at all dosage levels of zinc oxide nanoparticles. The zinc oxide nanoparticles promote complete combustion of the fuel charge when compared with biodiesel fuel blends. Equations (3) and (4) illustrates the estimation of BP and BTE, respectively:

$$BP = \frac{2\pi NT}{60000} = \frac{2\pi N(W \times R)}{60000} = \frac{0.785 \times N \times (W \times 9.81) \times Arm \ lenght}{60000} kW \qquad (3)$$

$$BTE = \frac{BP \times 3600 \times 100}{Fuel \ flow \left(\frac{kg}{hr}\right) \times Cv}\% \qquad (4)$$

Brake thermal efficiency for all tested fuels with different compression ratios at variable load is presented in Figure 7a,b. BTE increased with an increase in load up to 80%, then exhibited a slight reduction at 100% load. At maximum load and CR 21.5, the BTE increased by 11.592% (SBME25ZnO25), 23.2% (SBME25ZnO50), and 19.024% (SBME25ZnO75) compared to SBME25 fuel. Diesel fuel exhibited a BTE value that was 29.64% lower with 18.5 CR at 80% load. All fuel blends showed lower BTE values compared to diesel due to lower calorific value, lower brake power, and higher BSFC. In addition, the BTE value fell with a reduction in compression ratio. All tested fuels showed a reduction in BTE values: 9.88% (diesel), 15.4% (SBME25ZnO25), 6.15% (SBME25ZnO50), 11.1% (SBME25ZnO75), and 20.5% (SBME25) with a compression ratio of 18.5 compared to a CR of 21.5, due to lower compression temperature, which resulted in poor combustion of fuel. BTE is directly proportional to compression ratio [47]. Brake thermal efficiency showed an enhancement with an increase in loads and lower heat losses at higher engine load [48]. The metal zinc oxide nanoparticles improved the combustion process by reducing its duration and ignition delay, and increased in-cylinder temperature and pressure, and high HRR subsequently increased the BTE [49,50]. Zinc oxide nanoparticles act as a potential catalyst due to their high reactive surface area during the combustion process, which leads to a micro explosion of fuel droplets resulting in improved combustion characteristics, such as cylinder pressure and high heat release rate, therefore increasing the BTE.
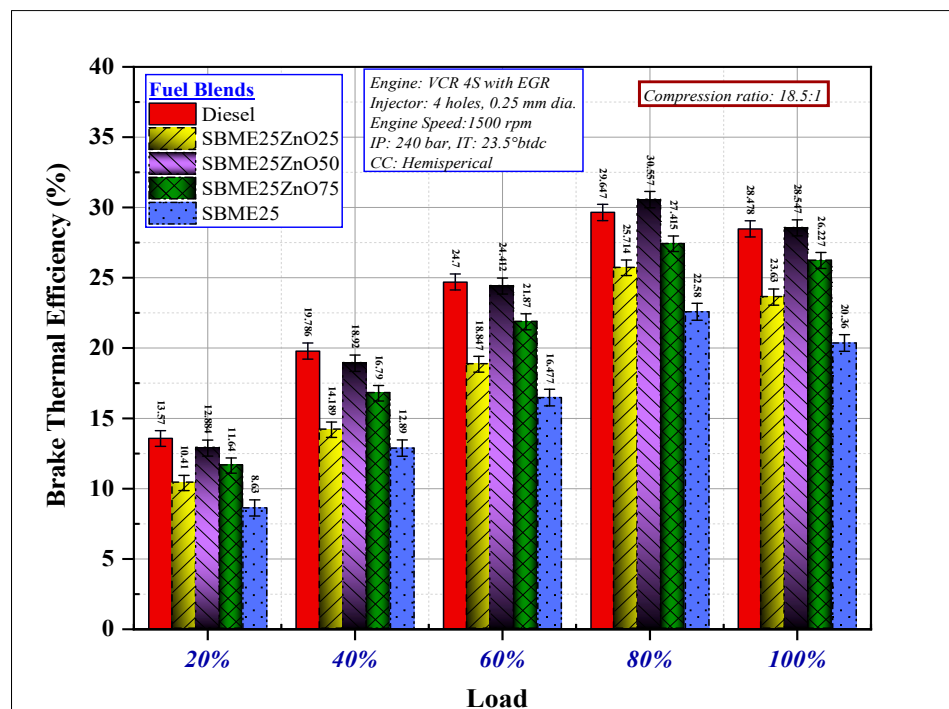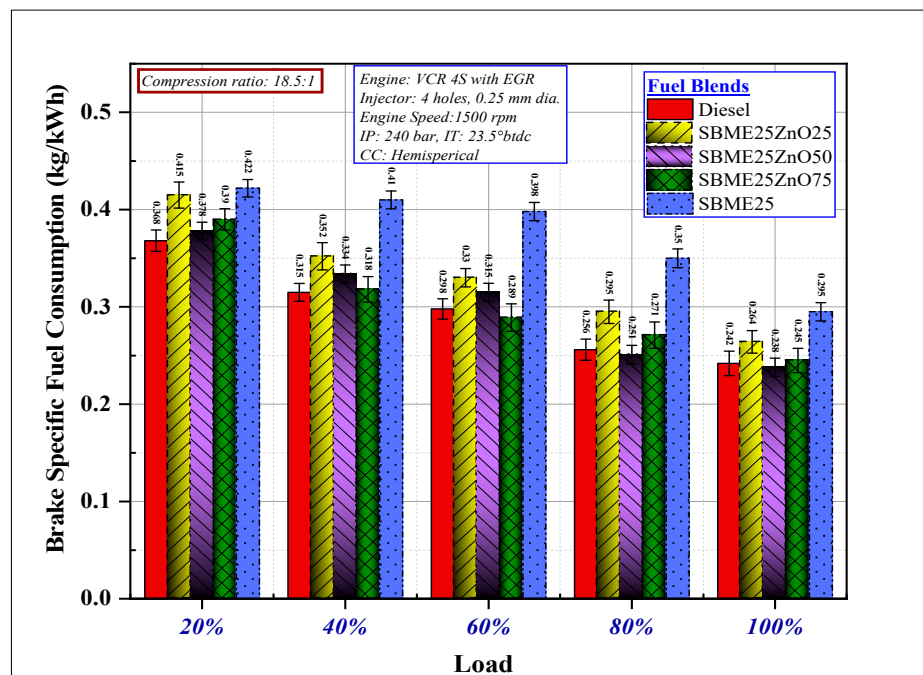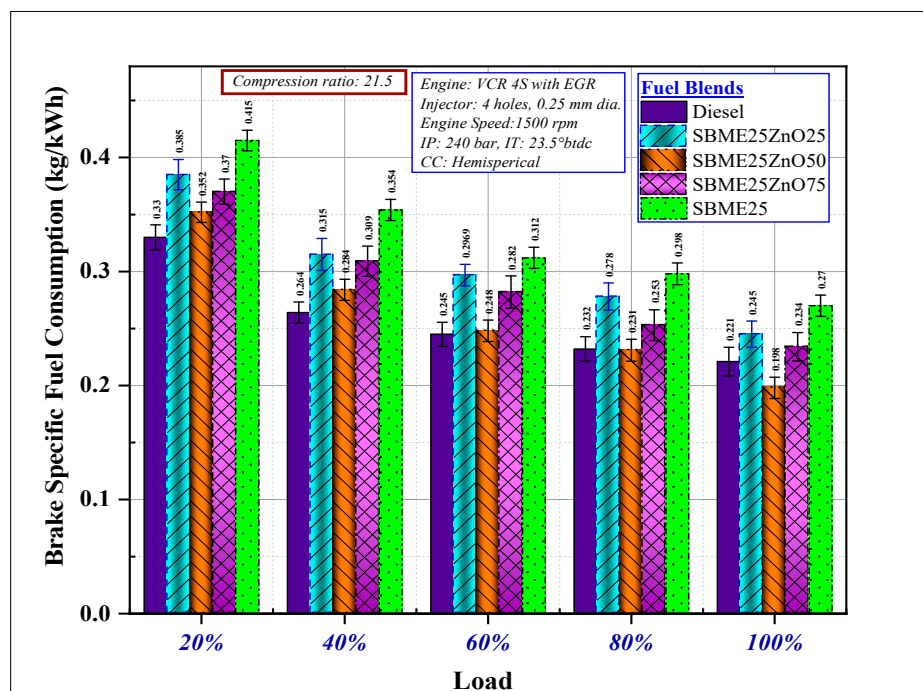
(**a**)
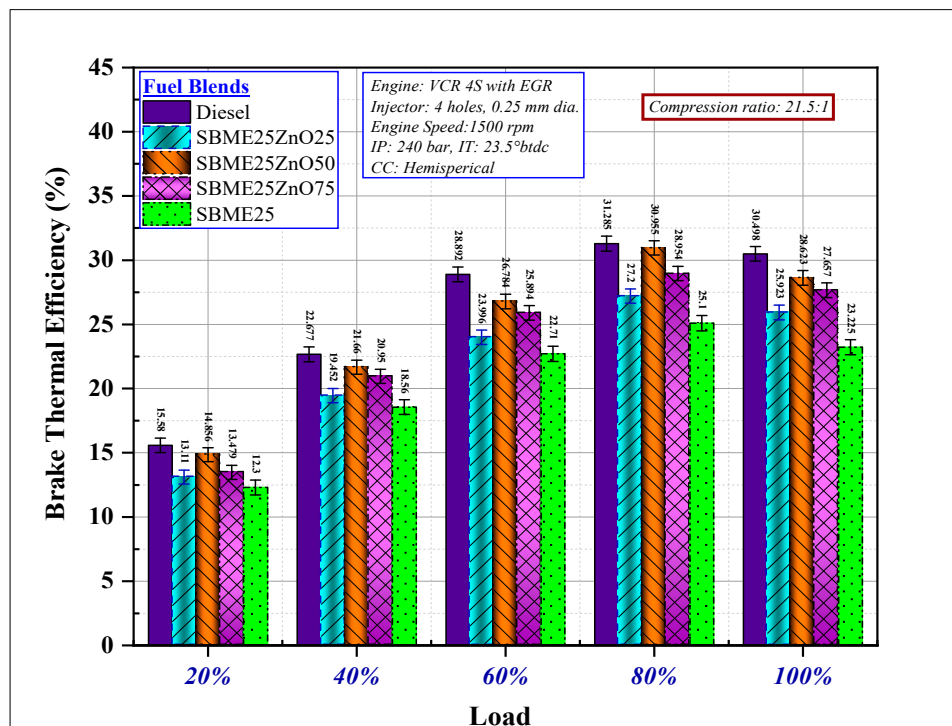
(**b**)

Figure 6. The variation of BTE at compression ratios of (**a**) 18.5 and (**b**) 21.5.

(**a**)

(**b**)

Figure 7. The variation of BTE at compression ratios: (**a**) 18.5 and (**b**) 21.5.

3.1.2. The Effect of SBME25-ZnO Nanofuel Blends on Brake Specific Fuel Consumption (BSFC) at Different Compression Ratios

Figure 7a,b show the variation of BSFC and loads for various fuel blends at different compression ratios. The BSFC is reduced with an increase in engine load. The lowest BSFC value with 21.5 CR 0.198 Kg/kWh for SBME25ZnO50 is obtained at 100% engine load. On average, the BSFC values were 0.258 Kg/kWh (diesel), 0.262 Kg/kWh (SBME25ZnO50), 0.2896 Kg/kWh (SBME25ZnO75), 0.304 Kg/kWh (SBME25ZnO25), and 0.329 Kg/kWh (SBME25) at 21.5 CR. All ternary fuel blends showed reduction in BSFC: 20.37%, 12.18%, and 7.82% for SBME25ZnO50, SBME25ZnO75, and SBME25ZnO25, respectively, compared to SBME25. The minimum BSFC value was recorded with zinc oxide (50 ppm) as a fuel additive. SBME25ZnO50 showed higher BSFC value 0.245 Kg/kWh with 18.5 compression ratio at 100% engine load. The average BSFC values for all tested fuels increased with a decrease in compression ratio. All tested fuels showed a rise in the BSFC for 18.5 compression ratio: 14.47% (diesel), 8.94% (SBME25ZnO25), 15.46% (SBME25ZnO50), 4.48% (SBME25ZnO75), and 13.7% (SBME25), compared to 21.5 compression ratio. At higher load, BSFC values are reduced due to less heat loses and a smaller amount of fuel is required to obtain specific brake power [51,52]. A similar increase in BSFC with an increase in compression ratio has been reported by various researchers [48,53,54]. Biodiesel with fuel additive (ZnO) showed significant reduction in BSFC due to improved combustion characteristics. Nanoparticle enhanced the air–fuel mixing, micro explosion of fuel droplets, and secondary atomization, resulting in lower BSFC. The combustion process is improved with the use of ZnO as a fuel additive (oxidizing agent) due to its high calorific value, shorter ignition delay, and more reactive surface area [49]. Dahad et al. [55] and Deepak et al. [56] reported a similar reduction in BSFC with the use of zinc oxide as a fuel additive in a diesel engine.

3.2. The Effect of Zinc Oxide Nano-Additives and Soybean Fuel Blend on Engine Emissions

3.2.1. The Effect of SBME25-ZnO Nanofuel Blends on Carbon Monoxide (CO) Emissions at Different Compression Ratios

The variation in carbon monoxide emissions and loads for all tested fuels at different compression ratio is presented in Figure 8a,b. Carbon monoxide emissions are produced due to incomplete combustion during the combustion process. All tested fuels showed reduction in carbon monoxide emissions, with the exception of diesel, due to the presence of extra oxygen molecules, which results in complete conversion of CO to CO_2 [57]. SBME25ZnO50 showed the lowest CO emissions among all tested fuels due to the presence of extra oxygen and reactive surface area (ZnO), which leads to high in-cylinder temperature and pressure resulting in complete combustion. On average, the CO emissions were reduced by 41.08%, 31.44%, and 18.66% for SBME25ZnO50, SBME25ZnO75, and SBME25ZnO25 ternary blends, respectively, compared to SBME25. All tested fuels showed an increase in CO emission values: 20.85% (diesel), 19.87% (SBME25ZnO25), 4.23% (SBME25ZnO50), 6.53% (SBME25ZnO75), and 14.45% (SBME25) with compression ratio of 18.5 compared to a compression ratio of 21.5. This was due to a lower compression temperature, which resulted in poor combustion of fuel. A similar result has been reported by Sharma et al. [58], in which an increase in the compression ratio resulted in an increased air temperature, leading to a reduction in the ignition delay period and CO emissions due to complete combustion.
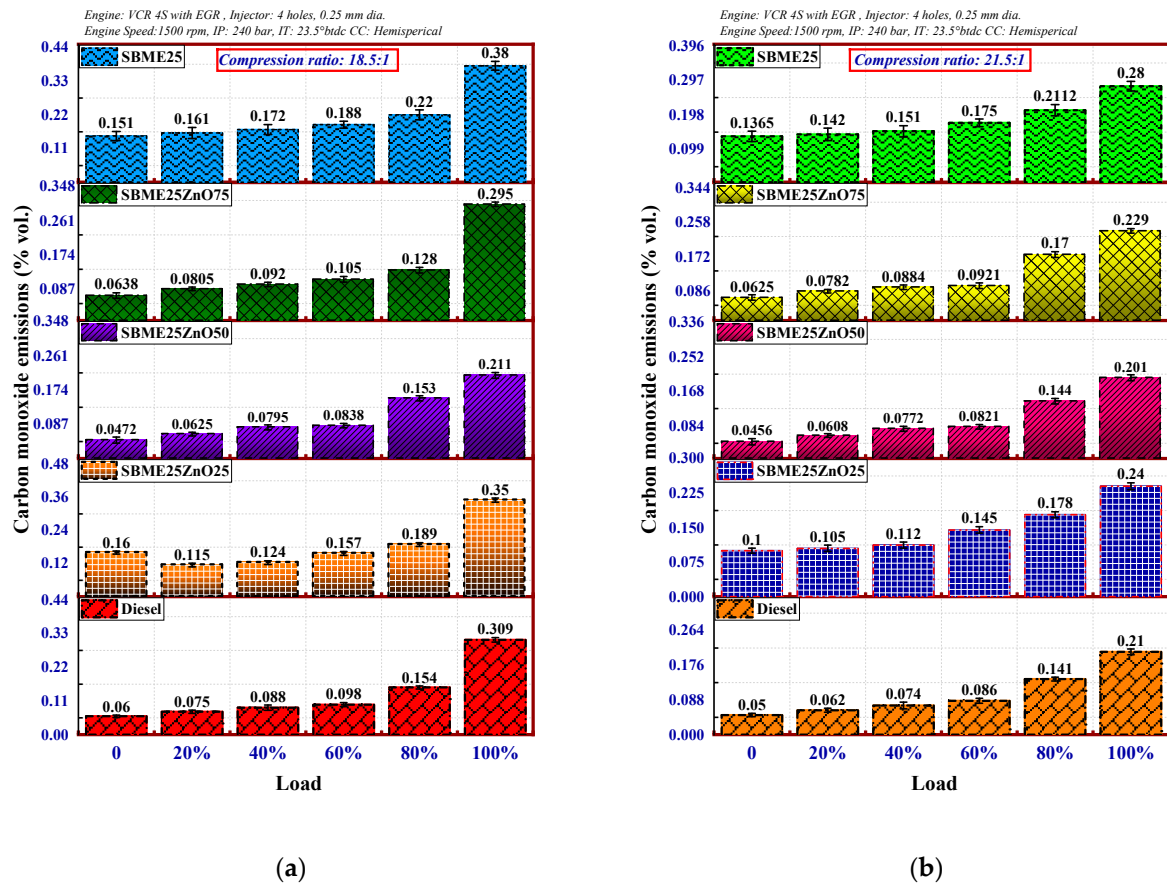
Figure 8. The variation of carbon monoxide at compression ratios: (**a**) 18.5 and (**b**) 21.5.

3.2.2. The Effect of SBME25-ZnO Nanofuel Blends on Hydrocarbon (HC) Emissions at Different Compression Ratios

HC emissions for diesel, SBME25ZnO25, SBME25ZnO50, SBME25ZnO75, and SBME25 at variable load with different compression ratios are shown in Figure 9a,b. HC emissions are mainly affected by fuel characteristics, fuel spray properties, and different engine operating conditions. The average HC emissions at CR 21.5 were 0.131, 0.139, 0.147, 0.1530, and 0.189 g/kWh for SBME25ZnO50, diesel, SBME25ZnO75, SBME25ZnO25, and SBME25, respectively, from minimum to maximum engine loads. All ternary fuel blends showed reduction in HC emissions compared to a neat biodiesel–diesel blend. Overall, significant reductions in HC emissions for a compression ratio of 21.5 of 30.83%, 22.12%, and 18.76% were observed for SBME25ZnO50, SBME25ZnO75, and SBME25ZnO25, respectively, compared to SBME25. The fuel blend SBME25 showed maximum HC emissions due to its viscous attributes, which resulted in poor fuel spray characteristics and led to incomplete combustion. All fuels tested at CR 18.5 showed higher HC emissions compared to CR 21.5. HC emissions are mainly affected by the air–fuel mixture and the air-to-fuel equivalence ratio from rich to lean mixture. A similar increase in HC emissions due to a lower compression ratio was reported by Sharma et al. [58]. All tested fuels showed an increase in CO emission values: 12.58% (diesel), 12.26% (SBME25ZnO25), 14.35% (SBME25ZnO50), 8.27% (SBME25ZnO75), and 20.48% (SBME25) with a compression ratio of 18.5 compared to 21.5 CR.
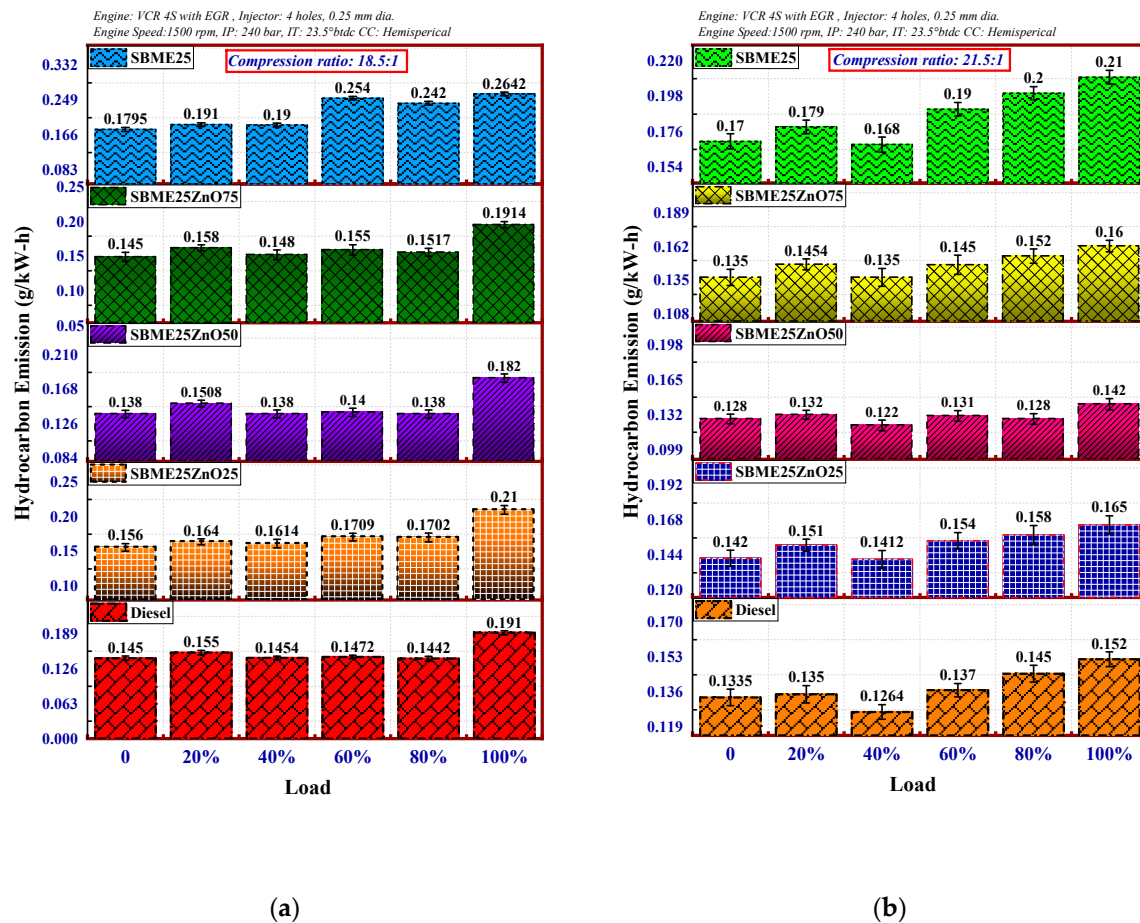
Figure 9. The variation of hydrocarbon emissions at compression ratios: (**a**) 18.5 and (**b**) 21.5.

3.2.3. The Effect of SBME25-ZnO Nanofuel Blends on Nitrogen Oxide (NOx) Emissions at Different Compression Ratios

NOx emissions for all tested fuels with variable loads and different compression ratios are presented in Figure 10a,b. NOx emissions increased with increase in engine load. High NOx emissions were generated due to high in-cylinder temperature resulting from complete combustion. Extra oxygen molecules in biodiesel and ternary blends enhanced the combustion process and resulted in the high in-cylinder pressure and temperature that leads to higher NOx emissions. Average NOx emissions at a compression ratio of 21.5 287.73, 290.77, 365.73, 412.51, and 456.14 ppm were obtained for SBME25, diesel, SBME25ZnO25, SBME25ZnO50, and SBME25ZnO75, respectively, between 20% and 100% engine loads. All ternary blends showed a slight increase in NOx emissions compared to diesel and biodiesel–diesel blends due to high in-cylinder temperature and pressure. NOx emissions were increased by 27.10%, 43.36% and 58.52% at 21.5 CR for SBME25ZnO25, SBME25ZnO50, and SBME25ZnO75, respectively, compared to SBME25. Ternary fuel blends improved the combustion process due to high oxygen content in fuel additives as well as in biodiesel, which leads to shorter ignition delay due to high cetane number [57,59]. At a compression ratio of 18.5, NOx emissions were reduced compared to the engine tested at a higher compression ratio of 21.5. The combustion temperature was increased due to a higher compression ratio because of the high oxygen intake that leads to improved combustion phenomena and results in higher NOx emissions.
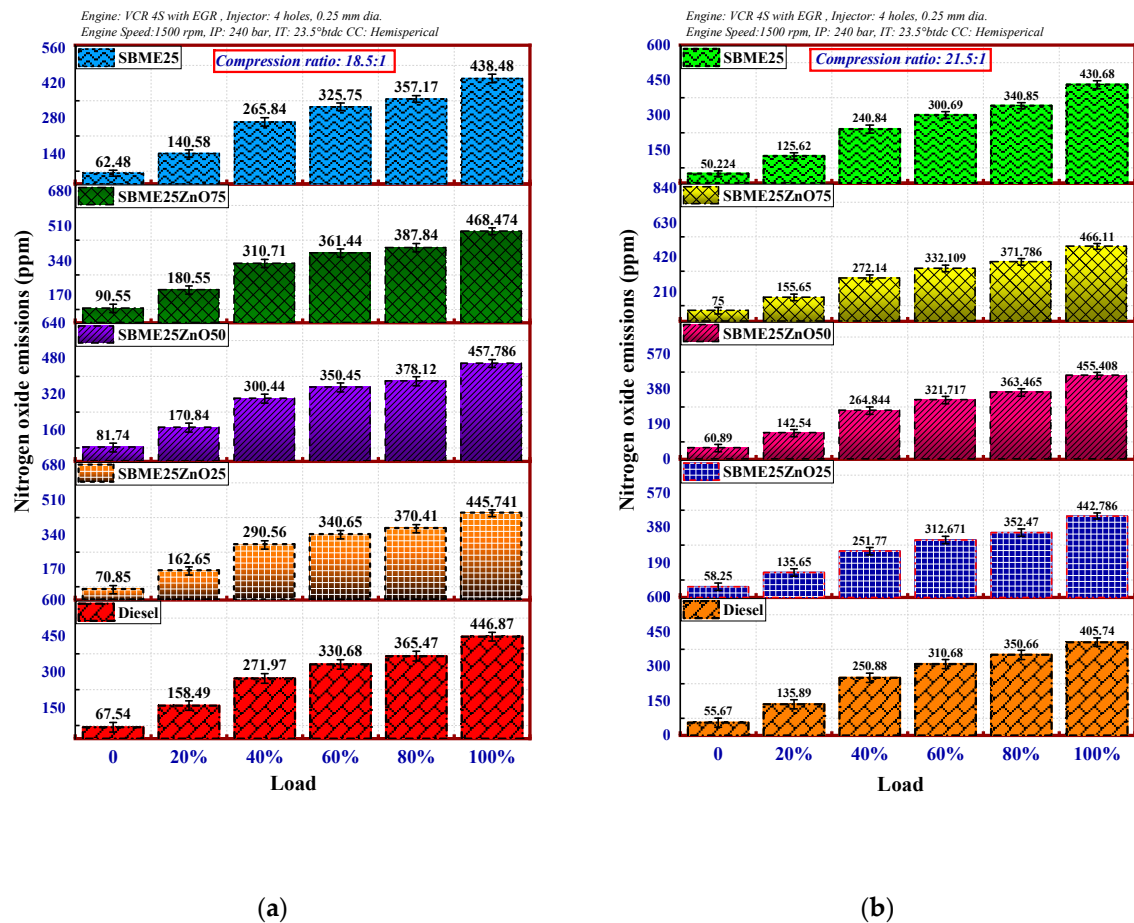
(**a**)   (**b**)

Figure 10. The variation of nitrogen oxide emissions at compression ratios: (**a**) 18.5 and (**b**) 21.5.

3.2.4. The Effect of SBME25-ZnO Nanofuel Blends on Carbon Dioxide (CO_2) Emissions at Different Compression Ratios

The carbon molecules from the fuel combustion combines with the oxygen to produce carbon dioxide emissions. Figure 11a,b show an increasing trend in CO_2 emissions with increasing loading conditions. For the compression ratio of 18.5, all the nanofuel blends lowered the carbon dioxide emissions due to complete fuel combustion and lower generation of carbon molecules post combustion process compared to the SBME25 fuel blend. In addition, a similar trend was observed for a compression ratio of 21.5, however, lower carbon dioxide emissions were observed at a higher compression ratio due to rapid combustion and enhanced micro-explosion process. At compression ratio of 21.5, fuel blend SBME25ZnO50 showed lower carbon dioxide emissions compared to all fuel blends at maximum load. The CO_2 for 50 ppm of ZnO in SNME25 was lower by 21.66% and 2.36%, respectively, compared to SBME25 and diesel fuel. This was due to the large surface area of ZnO nanoparticles enabling complete combustion of hydrocarbon molecules [59,60].
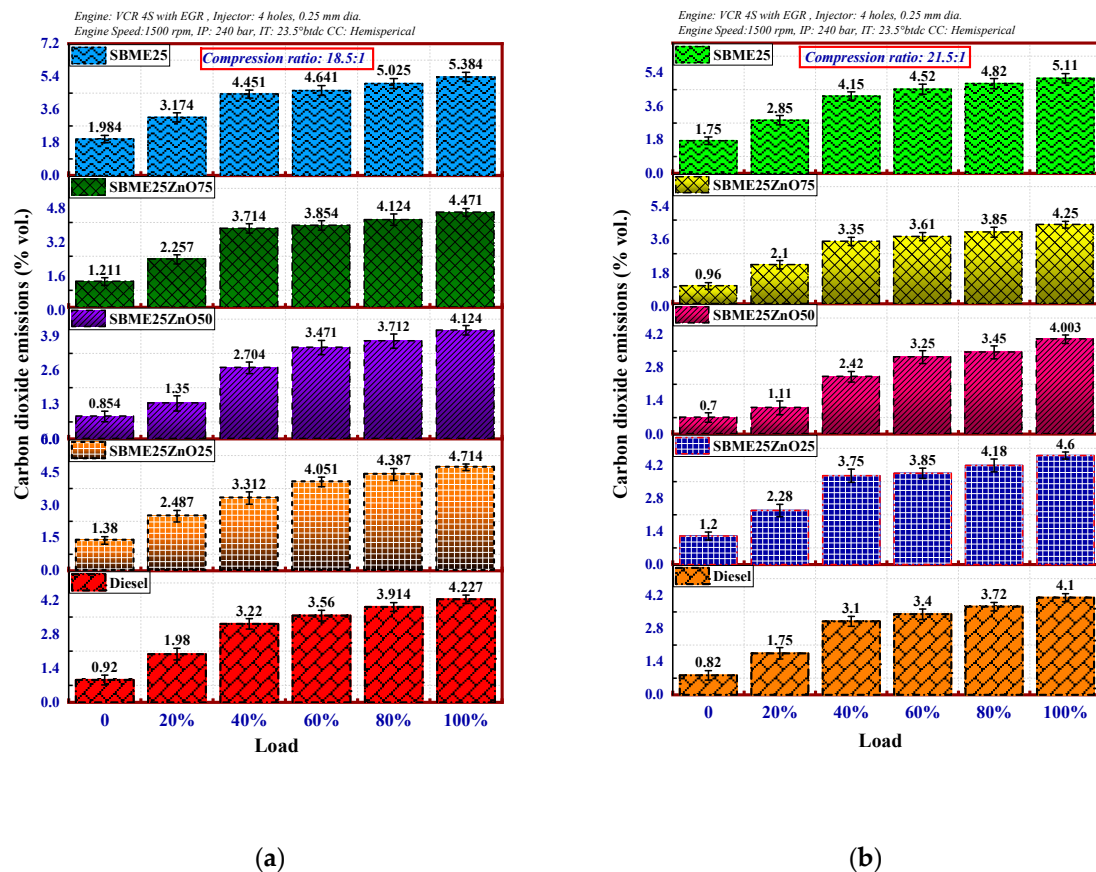
(**a**)   (**b**)

Figure 11. The variation of carbon dioxide emissions at compression ratios: (**a**) 18.5 and (**b**) 21.5.

3.2.5. The Effect of SBME25-ZnO Nanofuel Blends on Smoke Emissions at Different Compression Ratios

The smoke emissions for all tested fuels with variable loads and different compression ratios are illustrated in Figure 12. The smoke emissions are produced due to incomplete combustion of hydrocarbon particles in the combustion chamber, a rich air-to-fuel mixture, and poor fuel vaporization.

The SBME25 fuel blend produces higher smoke emissions due to lower calorific value and heat release rate. In contrast, the biodiesel blends with ZnO nanoparticles improved the micro-explosion phenomenon and air-to-fuel mixing, leading to lower smoke emissions. The smoke emissions for compression ratios of 18.5 and 21.5 for SBME25ZnO50 fell by 19.95% and 22.54%, respectively, compared with SBME25 and diesel fuel. The large surface area of the ZnO nanoparticles enhances the combustion process resulting in complete fuel combustion. An increase in the compression ratio leads to better air-to-fuel mixing and increases the temperature during the compression stroke. In addition, an increase in the compression ratio reduces the dilution of the fuel charge by residual gases [61].
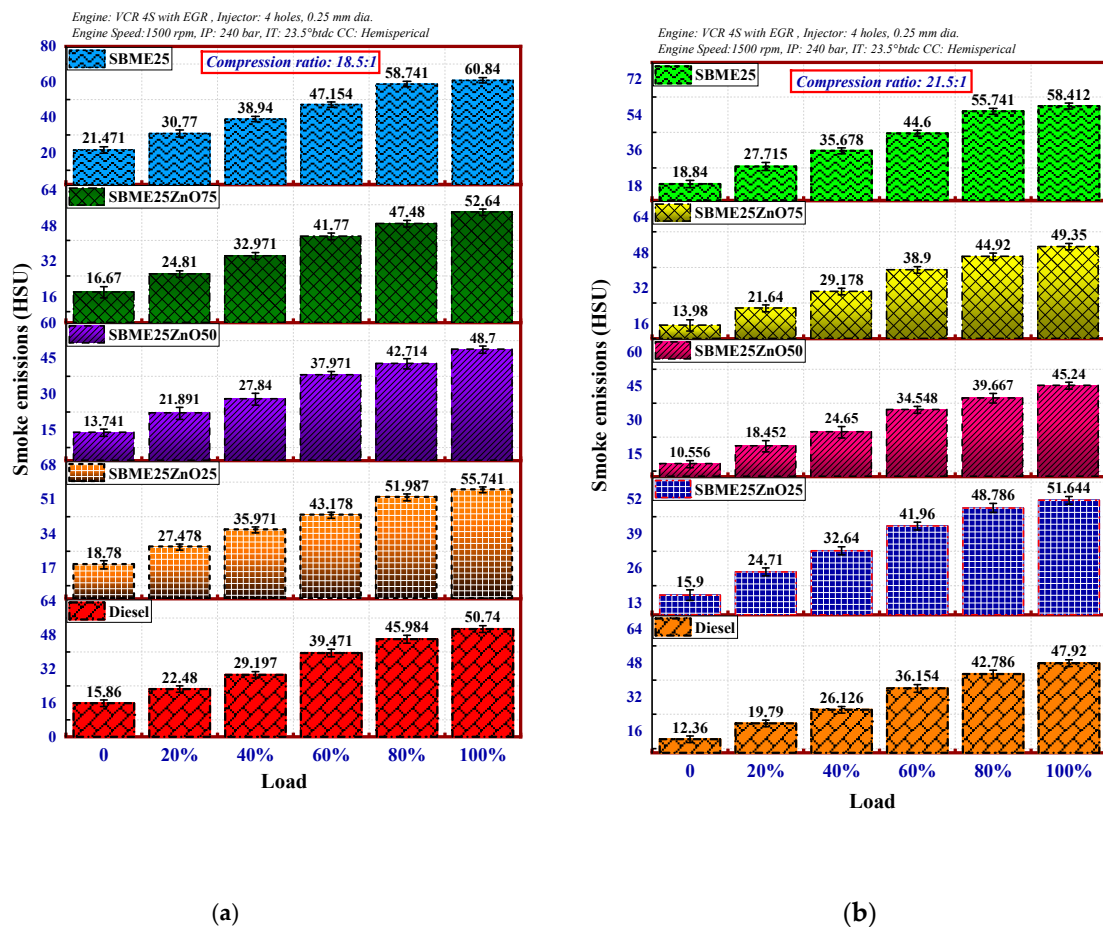
**Figure 12.** The variation of smoke emissions at compression ratios: (**a**) 18.5 and (**b**) 21.5.

3.3. The Effect of Zinc Oxide Nano-Additives and Soybean Fuel Blend on Engine Combustion Characteristics

3.3.1. The Effect of SBME25-ZnO Nanofuel Blends on Ignition Delay at Different Compression Ratios

The ignition delay period is a critical phenomenon from the perspectives of preparation of the fuel before being injected into the combustion chamber and selection of ideal injection timings. The ignition delay period of a diesel engine is the time period between the start of injection and start of combustion. The ignition delay period in the context of diesel engines is the period from the first charge of fuel entering the combustion chamber to the period when the first flame propagates [62]. The ignition delay period depends primarily on the ambient temperature. Due to fuel vaporization, the HRR curve shows negative values prior to the start of combustion for diesel engines.

As it is evident from Figure 13a,b that the ignition delay period reduces with an increase in the loading conditions due to a rise in the pressure and temperature for all the fuel blends. The rise in pressure results in the mixture of molecules coming closely together, enhancing the chemical reactions due to the active collisions of molecules, and resulting in a shorter ignition delay period. The higher viscosity of soybean biodiesel results in poor atomization of fuel droplets, air-to-fuel mixing, and lower flame cone angle, resulting in an increase in the delay period. The ZnO nanoparticles in SBME25 result in a reduction in the ignition delay period due to enhancement of combustion rate and better premixed combustion phase. At the higher compression ratio of 21.5, due to higher injection air-to-fuel mixture in the combustion chamber, at the same injection timing and injection pressure, the ignition delay period is lowered compared to 18.5 CR. At maximum load and compression ratio of 21.5, the values of ignition delay period for SBME25ZnO concentrations of 50, 75, and 25 ppm, respectively, were 7.21, 8.125 and 8.786 °CA, while at a compression ratio of 18.5 the values were 7.744, 8.125, and 9.174 °CA. At both compression ratios, the ignition delay period observed for SBMEZnO50 was lower than that of all the fuel blends. At a compression ratio of 21.5 for the SBMEZnO50 fuel blend, reductions of

25.02% and 5.38% were observed, and at a compression ratio 18.5, reductions of 23.47% and 2.18% were observed, compared to SBME25 and neat diesel, respectively. This was due to the high catalytic activity of zinc oxide nanoparticles, which enhance the combustion phenomena. However at higher proportions of ZnO in the fuel blends, the ignition delay period slightly increases due to a negligible increase in the viscosity.
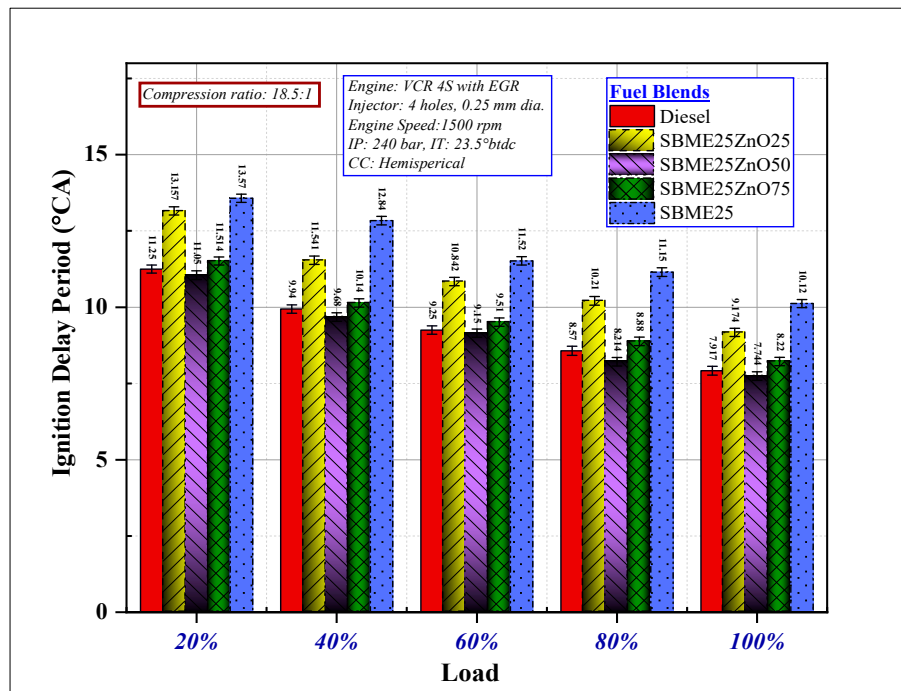
(**a**)
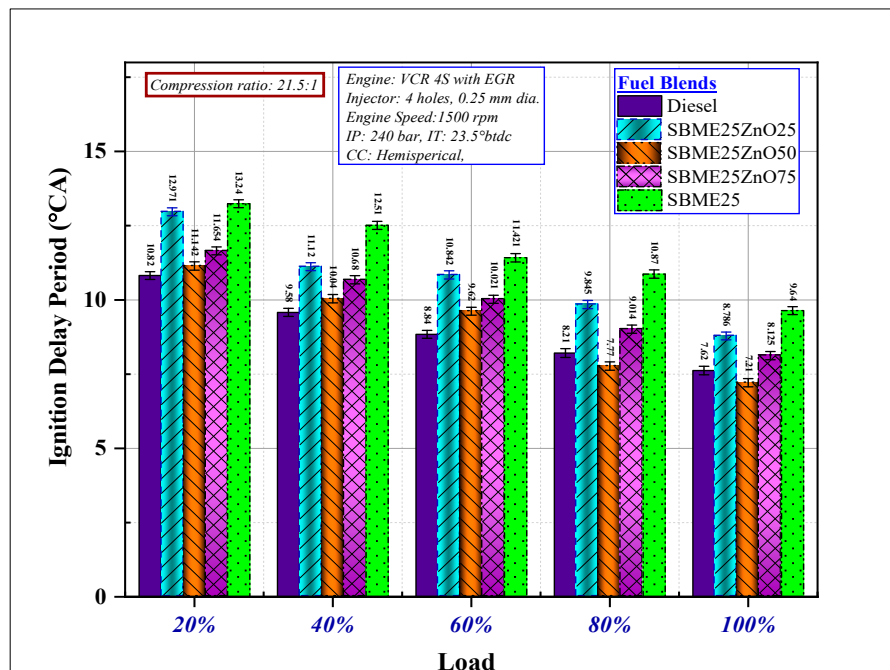
(**b**)

Figure 13. Variation of ignition delay period with load at compression ratios: (**a**) 18.5 and (**b**) 21.5.

3.3.2. The Effect of SBME25-ZnO Nanofuel Blends on Mean Gas Temperature at Different Compression Ratios

The mean value of the cylinder temperature of combusted and unburned gases present in the combustion chamber during a cycle is known as mean gas temperature. Figure 14 illustrates the mean gas temperature of fuel blends at varying crank angles at maximum load and compression ratio of 21.5. The gases present in the cylinder are the blend of combusted and unburned air–fuel mixture. The mean gas temperature ascertains the rate of combustion reaction of the fuel, and the desired value should be nearer to the adiabatic temperature of the flame. The adiabatic flame temperature is achieved when there is no loss in thermal energy and an adiabatic state is reached. At this point, maximum pressure is reached, although the process of combustion is incomplete, and the combustion continues for another few °CA in the boundary of the combustion chamber. Peaks in the mean gas temperature for all the fuel blends are observed from 370 to 385 °CA, and the mean gas temperature for diesel is 1334.29 °C at 380 °CA. The nanofuel blend, SBME25ZnO50, exhibited a mean cylinder temperature of 1329.11 °C at 379 °CA. Slightly lower values of mean gas temperature were observed for SBME25: the peak of 1301.87 °C was seen at 380 °CA due to viscosity and density.
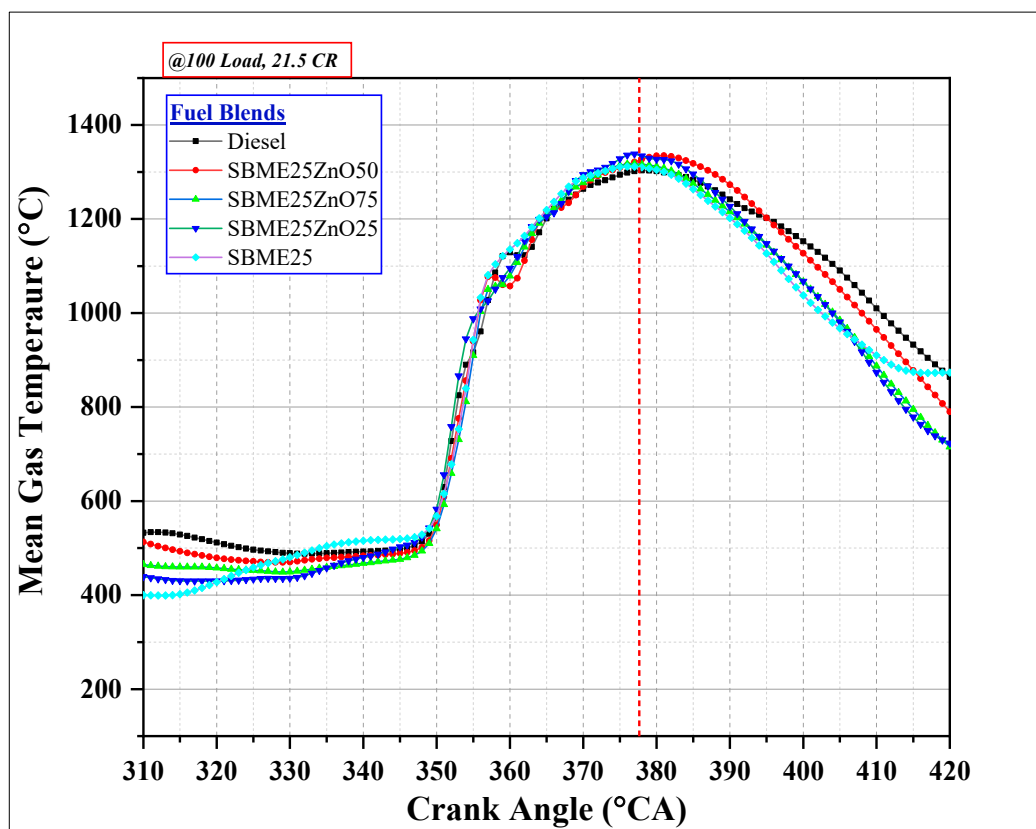

Figure 14. The mean gas temperature of fuel blends at varying crank angles at maximum load and CR 21.5.

3.3.3. The Effect of SBME25-ZnO Nanofuel Blends on Heat Release Rate at Different Compression Ratios

The first law of thermodynamics is used to evaluate the heat release rate (HRR), which is the decrease in heat transfer and mass at cylinder pressure, and effective variations in volume at a closed engine cycle. The contents of the cylinder are considered uniform with modeled properties in the thermodynamic state and characterized by average values. The model is considered as having zero dimension as no spatial variants are considered. In the current investigation, the experimental heat release rate is determined using the first law-single zone model illustrated in Equation (5):

$$\frac{dQ_n}{d\theta} = \frac{\gamma_h}{\gamma_h - 1} \times p\frac{dV}{d\theta} + \frac{1}{\gamma_h - 1} \times V\frac{dp}{d\theta} + \frac{dQ_w}{d\theta} \tag{5}$$

where T_m is the mean in-cylinder temperature. γ_h is the specific heat, shown in Equation (6):

$$\gamma_h = 1.35 - 6 \times 10^{-5} \times T_m + 10^{-8} \times T_{m^2} \tag{6}$$

In Figure 15a,b, the heat release rate is averaged over 400 cycles for a smooth curve and to avoid any irregularity in the combustion cycles that may occur in diesel engines fueled with low-ignition biofuels. The HRR is negative during the ignition delay period, due to the cooling effect caused by the vaporization of the fuel and loss of heat at the cylinder walls. Once the auto-ignition starts in the combustion process, the heat release rate becomes positive and a rapid growth in the peak is observed. The increase in the heat release rate for all the nanofuel blends is due to an enhanced cetane number and lower ignition delay period, which assist in increasing the efficiency of the engine. At a compression ratio of 21.5, all the fuel blends illustrated an enhancement in the heat release rate due to higher pressure and combustion rate, leading to complete burning of the fuel charge and resulting in higher energy output compared with the compression ratio of 18.5. The HRR for the SBME25 biodiesel blend was lower than the other fuel blends due to the high molecular weight and low burning velocity. The enhancement in heat release rate for the nanofuel blends is due to improved surface area, volume, high ignition properties, and thermal conductivity. The maximum peaks observed for SBME25 ZnO (25, 50, and 75 mg/L, respectively) at compression ratio 18.5 were 51.31, 58.97, and 62.26 J/°CA, while the peaks for diesel and SBME25 were 66.72 and 49.12 J/°CA, respectively. The compression ratio of 21.5 illustrated a higher HRR due to higher burning velocity of fuel blends; the HRR values for 25, 50, and 75 ppm of ZnO in SBME25 were 61.844, 70.44, and 65.854 J/°CA, respectively. The addition of zinc oxide nanoparticles in the SBME25 biodiesel blend increases the HRR at both compression ratios due to enhancement in oxygen content during combustion and atomization of fuel particles [33,56,60–65]. Table 7 illustrates the final results analysis of SBME25 and nanofuel blends.
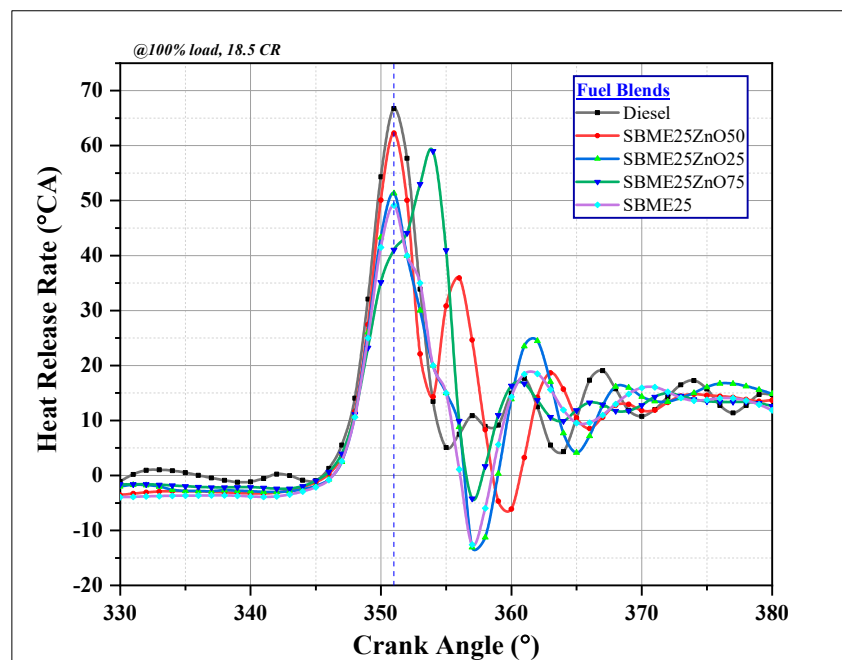
(**a**)
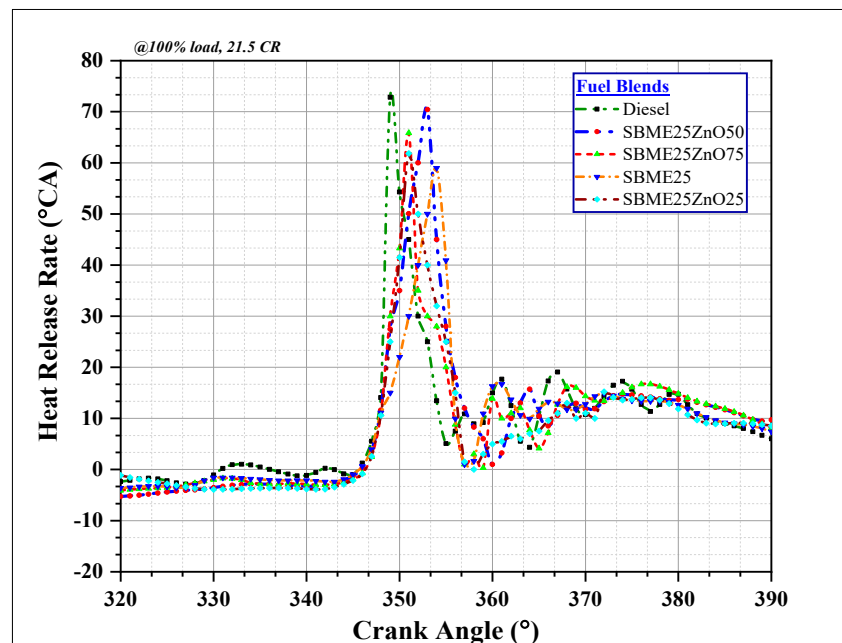
(**b**)

Figure 15. The variation of heat release rate with °CA at maximum load and compression ratios:
(**a**) 18.5 and (**b**) 21.5.

Table 7. The results analysis of SBME25 and nanofuel blends.

Color Code	Description	Engine Parameters	SBME25 CR 18.5	SBME25 CR 21.5	SBME25ZnO25 CR 18.5	SBME25ZnO25 (%)	SBME25ZnO25 CR 21.5	SBME25ZnO25 (%)	SBME25ZnO50 CR 18.5	SBME25ZnO50 (%)	SBME25ZnO50 CR 21.5	SBME25ZnO50 (%)	SBME25ZnO75 CR 18.5	SBME25ZnO75 (%)	SBME25ZnO75 CR 21.5	SBME25ZnO75 (%)
	CR 18.5	BSFC (kg/kWh)	0.295	0.27	0.264	10.508	0.245	9.25	0.238	19.322	0.198	26.66	0.245	16.94	0.234	13.33
		BTE (%)	20.36	23.23	23.63	16.56	25.923	11.592	28.547	40.211	28.62	23.2	26.277	28.86	27.65	19.024
	CR 21.5	CO (% vol.)	0.38	0.28	0.35	7.895	0.24	14.28	0.211	44.47	0.201	28.21	0.295	22.36	0.229	18.21
		HC (g/kWh)	0.2642	0.21	0.21	20.514	0.165	21.45	0.182	31.112	0.142	32.234	0.1914	27.55	0.16	23.807
	Decreases	CO_2 (% vol.)	5.384	5.11	4.714	12.44	4.6	9.98	4.471	23.402	4.003	21.66	4.124	16.951	4.25	16.82
		NOx (ppm)	438.48	430.68	445.741	1.62	442.786	2.27	457.786	4.235	455.408	5.414	468.474	6.128	466.11	7.601
	Negative Rise	Smoke (HSU)	60.84	58.412	55.741	8.334	51.644	11.58	48.7	19.954	45.24	22.55	52.64	13.477	49.35	15.55
		ID (°CA)	10.12	9.64	9.174	9.347	8.786	9.72	7.744	23.47	7.21	26.2	8.22	19.74	8.125	18.64
	Increases	HRR (°CA)	49.125	58.97	51.312	4.426	61.844	4.841	62.26	26.715	70.44	19.45	58.97	20.972	65.854	11.6
		MGT (°K)	-	1303.36	-	-	1311.97	0.66	-	-	1334.72	2.406	-	-	1317.22	1.06

4. Conclusions

The present study focuses on the effects of zinc oxide nanoparticles and soybean biodiesel blends at different loads and varying CRs on a VCR, single cylinder engine with IT of 23°BTDC and at a constant speed 1500 rpm. In the investigation, the engine was operated at two compression ratios of 18.5 and 21.5. Three nanofuel blends, SBME25ZnO25, SBME25ZnO50, and SBME25ZnO75, were prepared using the ultrasonication process by varying the dosage levels of ZnO nanoparticles and sodium dodecyl sulfate (SDS) surfactant. The following conclusions are drawn based on the obtained results:

1. The addition of ZnO nanoparticles to SBME25 enhanced the fuel properties, such as the calorific value and cetane number, while the density and viscosity were comparable to SBME25.
2. The performance characteristics of the VCR engine were enhanced for the ternary fuel blends. The dosage level of 50 ppm in SBME25 biodiesel and compression ratio of 21.5 increased the BTE by 20.59% and reduced the BSFC by 20.37% compared with the SBME25 fuel blend due to enhanced catalytic activity of zinc oxide nanoparticles.
3. The heat release rate and mean gas temperature of SBME25ZnO50 were comparable with diesel fuel. The enhancement in the heat release rate is due to the micro-explosion phenomenon occurring in the combustion chamber.
4. Emissions decreased with the addition of ZnO nanoparticles in the fuel blends. HC, CO, smoke, and CO_2 emissions were reduced by 30.83%, 41.08%, 22.54%, and 21.66%, respectively. NOx emissions increased slightly due to excess oxygen in the combustion chamber.

The results and conclusion validate that ZnO nanoparticles in soybean biodiesel at a CR of 21.5 enhance performance and combustion, and reduce the emissions of a common rail direct injection engine.

5. Recommendations for Future Research

Based on a recent comprehensive review of the effect of the addition of nanoparticles to fuel blends on diesel engine characteristics by Soudagar et al. [1], the future research topics are suggested as follows:

1. An extensive investigation of the surface reaction and engine wear on engine parts, such as the combustion chamber, piston and piston rings, cylinder and cylinder linings, fuel injectors and exhaust pipe, is required to confirm the reliability of nano-additives in a diesel engine.
2. The impact of metal-based nanoparticles used as fuel additives in diesel/biodiesel fuel on human health should be examined before commercialization of the technology.
3. There is scope for further research on the effects of nanoparticles in exhaust emissions. This may raise an issue related to environmental pollution caused by the addition of nanoparticles to diesel and bio-diesel fuels.
4. Analysis of the cost and complexity in the preparation of nanoparticles, encompassing public safety and economic feasibility, should be considered in future research. Furthermore, efforts should be made in developing cost-effective and efficient nanoparticles.

Nomenclature

NPs	**Nanoparticles**
CRDI	Common rail direct injection
CI	Compression ignition
nm	Nanometer
g/kWh	Grams per kilowatt hour
CC	Combustion chamber
ATDC	After top dead center
FFA	Free fatty acid
ASTM	American Society for Testing and Materials
ID	Injection delay
CO₂	Carbon dioxide
NOₓ	Oxides of nitrogen
BTE	Brake thermal efficiency
SFC	Specific fuel consumption
IP	Injection pressure
EGT	Exhaust gas temperature
°CA	Crank angle (degrees)
SBME	Soybean methyl ester (Soybean biodiesel)
SBME25	SBME25 and 25 ppm
ZnO25	ZnO NPs
SBME25	SBME25 and 75 ppm
ZnO75	ZnO NPs
ZnO	**Zinc oxide**
SDS	Sodium dodecyl sulfate
IC	Internal combustion
ppm	Parts per million
m	Meter
HCC	Hemispherical combustion chamber
BTDC	Before top dead center
CR	Compression ratio
PP	Peak pressure
HC	Hydrocarbon
CO	Carbon monoxide
PM	Particulate matter
BSFC	Brake specific fuel consumption
T$_w$	Wall temperature
IT	Injection timing
HRR	Heat release rate
D100	100% diesel
SBME25	25% Soybean methyl ester blended with diesel
SBME25	SBME25 and 50 ppm
ZnO50	ZnO NPs

References

1. Soudagar, M.E.M.; Nik-Ghazali, N.N.; Kalam, M.A.; Badruddin, I.; Banapurmath, N.; Akram, N. The effect of nano-additives in diesel-biodiesel fuel blends: A comprehensive review on stability, engine performance and emission characteristics. *Energy Convers. Manag.* **2018**, *178*, 146–177. [CrossRef]

2. Soudagar, M.E.M.; Kittur, P.; Parmar, F.; Batakatti, S.; Kulkarni, P.; Kallannavar, V. Production of Mahua Oil Ethyl Ester (MOEE) and its Performance test on four stroke single cylinder VCR engine. In Proceedings of the IOP Conference Series: Materials Science and Engineering, Seoul, Korea, 26–28 May 2017; p. 012029.

3. Ovando-Medina, I.; Espinosa-García, F.; Núñez-Farfán, J.; Salvador-Figueroa, M. Does biodiesel from Jatropha curcas represent a sustainable alternative energy source? *Sustainability* **2009**, *1*, 1035–1041. [CrossRef]

4. Imran, S.; Korakianitis, T.; Shaukat, R.; Farooq, M.; Condoor, S.; Jayaram, S. Experimentally tested performance and emissions advantages of using natural-gas and hydrogen fuel mixture with diesel and rapeseed methyl ester as pilot fuels. *Appl. Energy* **2018**, *229*, 1260–1268. [CrossRef]

5. Mujtaba, M.; Cho, H.M.; Masjuki, H.; Kalam, M.; Ong, H.; Gul, M.; Harith, M.; Yusoff, M. Critical review on sesame seed oil and its methyl ester on cold flow and oxidation stability. *Energy Rep.* **2020**, *6*, 40–54. [CrossRef]

6. Delvi, M.K.; Soudagar, M.E.M.; Khan, H.; Ahmed, Z.; Shariff, I.M. Biodiesel Production Utilizing Diverse Sources, Classification of Oils and Their Esters, Performance and Emission Characteristics: A Research. *IJRTE* **2020**.

7. Soudagar, M.E.M.; Nik-Ghazali, N.N.; Kalam, M.; Badruddin, I.A.; Banapurmath, N.; Khan, T.Y.; Bashir, M.N.; Akram, N.; Farade, R.; Afzal, A. The effects of graphene oxide nanoparticle additive stably dispersed in dairy scum oil biodiesel-diesel fuel blend on CI engine: Performance, emission and combustion characteristics. *Fuel* **2019**, *257*, 116015. [CrossRef]

8. Sarafraz, M.; Jafarian, M.; Arjomandi, M.; Nathan, G. Potential use of liquid metal oxides for chemical looping gasification: A thermodynamic assessment. *Appl. Energy* **2017**, *195*, 702–712. [CrossRef]

9. Soudagar, M.; Afzal, A.; Kareemullah, M. Waste coconut oil methyl ester with and without additives as an alternative fuel in diesel engine at two different injection pressures. *Energy Sources Part A Recovery Util. Environ. Eff.* **2020**. [CrossRef]

10. Sarafraz, M. Experimental Investigation on Pool Boiling Heat Transfer to Formic Acid, Propanol and 2-Butanol Pure Liquids under the Atmospheric Pressure. *J. Appl. Fluid Mech.* **2013**, *6*, 73–79.

11. Sarafraz, M.; Hormozi, F.; Kamalgharibi, M. Sedimentation and convective boiling heat transfer of CuO-water/ethylene glycol nanofluids. *Heat Mass Transf.* **2014**, *50*, 1237–1249. [CrossRef]

12. Tamilvanan, A.; Balamurugan, K.; Ponappa, K.; Kumar, B.M. Copper nanoparticles: Synthetic strategies, properties and multifunctional application. *Int. J. Nanosci.* **2014**, *13*, 1430001. [CrossRef]

13. Farade, R.A.; Wahab, N.I.B.A.; Mansour, D.E.A.; Azis, N.B.; Banapurmath, N.; Soudagar, M.E.M. Investigation of the dielectric and thermal properties of non-edible cottonseed oil by infusing h-BN nanoparticles. *IEEE Access* **2020**. [CrossRef]

14. Akram, N.; Sadri, R.; Kazi, S.; Zubir, M.N.M.; Ridha, M.; Ahmed, W.; Soudagar, M.E.M.; Arzpeyma, M. A comprehensive review on nanofluid operated solar flat plate collectors. *J. Therm. Anal. Calorim.* **2020**, *139*, 1309–1343.

15. Peyghambarzadeh, S.; Sarafraz, M.; Vaeli, N.; Ameri, E.; Vatani, A.; Jamialahmadi, M. Forced convective and subcooled flow boiling heat transfer to pure water and n-heptane in an annular heat exchanger. *Ann. Nucl. Energy* **2013**, *53*, 401–410. [CrossRef]

16. Sarafraz, M.; Arjomandi, M. Thermal performance analysis of a microchannel heat sink cooling with copper oxide-indium (CuO/In) nano-suspensions at high-temperatures. *Appl. Therm. Eng.* **2018**, *137*, 700–709. [CrossRef]

17. Sarafraz, M.; Arjomandi, M. Demonstration of plausible application of gallium nano-suspension in microchannel solar thermal receiver: Experimental assessment of thermo-hydraulic performance of microchannel. *Int. Commun. Heat Mass Transf.* **2018**, *94*, 39–46. [CrossRef]

18. Sarafraz, M.; Arya, A.; Nikkhah, V.; Hormozi, F. Thermal performance and viscosity of biologically produced silver/coconut oil nanofluids. *Chem. Biochem. Eng. Q.* **2016**, *30*, 489–500. [CrossRef]

19. Sarafraz, M.; Peyghambarzadeh, S. Experimental study on subcooled flow boiling heat transfer to water–diethylene glycol mixtures as a coolant inside a vertical annulus. *Exp. Therm. Fluid Sci.* **2013**, *50*, 154–162. [CrossRef]

20. Saxena, V.; Kumar, N.; Saxena, V.K. A comprehensive review on combustion and stability aspects of metal nanoparticles and its additive effect on diesel and biodiesel fuelled CI engine. *Renew. Sustain. Energy Rev.* **2017**, *70*, 563–588. [CrossRef]

21. El-Seesy, A.I.; Abdel-Rahman, A.K.; Bady, M.; Ookawara, S. Performance, combustion, and emission characteristics of a diesel engine fueled by biodiesel-diesel mixtures with multi-walled carbon nanotubes additives. *Energy Convers. Manag.* **2017**, *135*, 373–393. [CrossRef]

22. Vellaiyan, S. Enhancement in combustion, performance, and emission characteristics of a diesel engine fueled with diesel, biodiesel, and its blends by using nanoadditive. *Environ. Sci. Pollut. Res.* **2019**, *26*, 9561–9573.

23.　Akram, N.; Sadri, R.; Kazi, S.; Ahmed, S.; Zubir, M.; Ridha, M.; Soudagar, M.; Ahmed, W.; Arzpeyma, M.; Tong, G.B. An experimental investigation on the performance of a flat-plate solar collector using eco-friendly treated graphene nanoplatelets–water nanofluids. *J. Therm. Anal. Calorim.* **2019**, *138*, 609–621.

24.　Kumar, S.; Dinesha, P.; Bran, I. Influence of nanoparticles on the performance and emission characteristics of a biodiesel fuelled engine: An experimental analysis. *Energy* **2017**, *140*, 98–105.

25.　Prabakaran, B.; Udhoji, A. Experimental investigation into effects of addition of zinc oxide on performance, combustion and emission characteristics of diesel-biodiesel-ethanol blends in CI engine. *Alex. Eng. J.* **2016**, *55*, 3355–3362.

26.　Venu, H.; Raju, V.D.; Subramani, L. Combined effect of influence of nano additives, combustion chamber geometry and injection timing in a DI diesel engine fuelled with ternary (diesel-biodiesel-ethanol) blends. *Energy* **2019**, *174*, 386–406.

27.　Basha, J.S. Impact of Carbon Nanotubes and Di-Ethyl Ether as additives with biodiesel emulsion fuels in a diesel engine–An experimental investigation. *J. Energy Inst.* **2018**, *91*, 289–303.

28.　Selvan, V.A.M.; Anand, R.; Udayakumar, M. Effect of Cerium Oxide Nanoparticles and Carbon Nanotubes as fuel-borne additives in Diesterol blends on the performance, combustion and emission characteristics of a variable compression ratio engine. *Fuel* **2014**, *130*, 160–167.

29.　Ashok, B.; Nanthagopal, K.; Mohan, A.; Johny, A.; Tamilarasu, A. Comparative analysis on the effect of zinc oxide and ethanox as additives with biodiesel in CI engine. *Energy* **2017**, *140*, 352–364.

30.　Venu, H. An experimental assessment on the influence of fuel-borne additives on ternary fuel (diesel–biodiesel–ethanol) blends operated in a single cylinder diesel engine. *Environ. Sci. Pollut. Res.* **2019**, *26*, 14660–14672.

31.　Özgür, T.; Özcanli, M.; Aydin, K. Investigation of nanoparticle additives to biodiesel for improvement of the performance and exhaust emissions in a compression ignition engine. *Int. J. Green Energy* **2015**, *12*, 51–56.

32.　Soudagar, M.E.M.; Nik-Ghazali, N.N.; Kalam, M.; Badruddin, I.A.; Banapurmath, N.; Ali, M.A.B.; Kamangar, S.; Cho, H.M.; Akram, N. An investigation on the influence of aluminium oxide nano-additive and honge oil methyl ester on engine performance, combustion and emission characteristics. *Renew. Energy* **2020**, *146*, 2291–2307.

33.　Karthikeyan, S.; Elango, A.; Prathima, A. Diesel engine performance and emission analysis using canola oil methyl ester with the nano sized zinc oxide particles. *Indian J. Eng. Mater. Sci.* **2014**, *21*, 83–87.

34.　Venu, H.; Madhavan, V. Effect of diethyl ether and Al_2O_3 nano additives in diesel-biodiesel-ethanol blends: Performance, combustion and emission characteristics. *J. Mech. Sci. Technol.* **2017**, *31*, 409–420.

35.　Sajith, V.; Sobhan, C.; Peterson, G. Experimental investigations on the effects of cerium oxide nanoparticle fuel additives on biodiesel. *Adv. Mech. Eng.* **2010**, *2*, 581407.

36.　Keskin, A.; Gürü, M.; Altıparmak, D. Influence of metallic based fuel additives on performance and exhaust emissions of diesel engine. *Energy Convers. Manag.* **2011**, *52*, 60–65.

37.　Mei, D.; Li, X.; Wu, Q.; Sun, P. Role of cerium oxide nanoparticles as diesel additives in combustion efficiency improvements and emission reduction. *J. Energy Eng.* **2016**, *142*, 04015050.

38.　Wu, Q.; Xie, X.; Wang, Y.; Roskilly, T. Effect of carbon coated aluminum nanoparticles as additive to biodiesel-diesel blends on performance and emission characteristics of diesel engine. *Appl. Energy* **2018**, *221*, 597–604.

39.　Emerging, S.C.O.; Risks, N.I.H. *The Appropriateness of Existing Methodologies to Assess the Potential Risks Associated with Engineered and Adventitious Products of Nanotechnologies*; European Commission Health and Consumer Protection Directorate-General: Brussels, Belgium, 2006; Volume 10.

40.　Haniffa, M.A.C.M.; Ching, Y.C.; Chuah, C.H.; Ching, K.Y.; Liou, N.S. Synergistic effect of (3-Aminopropyl) Trimethoxysilane treated ZnO and corundum nanoparticles under UV-irradiation on UV-cutoff and IR-absorption spectra of acrylic polyurethane based nanocomposite coating. *Polym. Degrad. Stab.* **2019**, *159*, 205–216.

41.　Li, Y.Q.; Fu, S.Y.; Mai, Y.W. Preparation and characterization of transparent ZnO/epoxy nanocomposites with high-UV shielding efficiency. *Polymer* **2006**, *47*, 2127–2132.

42.　Wahab, R.; Ansari, S.; Seo, H.K.; Kim, Y.S.; Suh, E.K.; Shin, H.S. Low temperature synthesis and characterization of rosette-like nanostructures of ZnO using solution process. *Solid State Sci.* **2009**, *11*, 439–443.

43.　Cao, D.; Gong, S.; Shu, X.; Zhu, D.; Liang, S. Preparation of ZnO nanoparticles with high Dispersibility based on oriented attachment (OA) process. *Nanoscale Res. Lett.* **2019**, *14*, 210. [PubMed]

44. Talam, S.; Karumuri, S.R.; Gunnam, N. Synthesis, characterization, and spectroscopic properties of ZnO nanoparticles. *ISRN Nanotechnol.* **2012**, *2012*, 1–6.

45. Bian, S.W.; Mudunkotuwa, I.A.; Rupasinghe, T.; Grassian, V.H. Aggregation and dissolution of 4 nm ZnO nanoparticles in aqueous environments: Influence of pH, ionic strength, size, and adsorption of humic acid. *Langmuir* **2011**, *27*, 6059–6068. [PubMed]

46. Moffat, R.J. Describing the uncertainties in experimental results. *Exp. Therm. Fluid Sci.* **1988**, *1*, 3–17.

47. Pushparaj, T.; Ramabalan, S. Green fuel design for diesel engine, combustion, performance and emission analysis. *Procedia Eng.* **2013**, *64*, 701–709.

48. Rosha, P.; Mohapatra, S.K.; Mahla, S.K.; Cho, H.; Chauhan, B.S.; Dhir, A. Effect of compression ratio on combustion, performance, and emission characteristics of compression ignition engine fueled with palm (B20) biodiesel blend. *Energy* **2019**, *178*, 676–684.

49. Khalife, E.; Tabatabaei, M.; Demirbas, A.; Aghbashlo, M. Impacts of additives on performance and emission characteristics of diesel engines during steady state operation. *Prog. Energy Combust. Sci.* **2017**, *59*, 32–78.

50. Mehta, R.N.; Chakraborty, M.; Parikh, P.A. Nanofuels: Combustion, engine performance and emissions. *Fuel* **2014**, *120*, 91–97.

51. Raheman, H.; Ghadge, S. Performance of diesel engine with biodiesel at varying compression ratio and ignition timing. *Fuel* **2008**, *87*, 2659–2666.

52. Soudagar, M.E.M.; Nik-Ghazali, N.N.; Badruddin, I.A.; Kalam, M.; Kittur, M.I.; Akram, N.; Ullah, M.A.; Khan, T.Y.; Mokashi, I. Production of honge oil methyl ester (HOME) and its performance test on four stroke single cylinder VCR engine. In Proceedings of the AIP Conference Proceedings, New Delhi, India, 6–7 March 2019; p. 200006.

53. Bora, B.J.; Saha, U.K. Experimental evaluation of a rice bran biodiesel–biogas run dual fuel diesel engine at varying compression ratios. *Renew. Energy* **2016**, *87*, 782–790.

54. Sayin, C.; Gumus, M. Impact of compression ratio and injection parameters on the performance and emissions of a DI diesel engine fueled with biodiesel-blended diesel fuel. *Appl. Therm. Eng.* **2011**, *31*, 3182–3188.

55. Dhahad, H.A.; Chaichan, M.T. The impact of adding nano-Al_2O_3 and nano-ZnO to Iraqi diesel fuel in terms of compression ignition engines' performance and emitted pollutants. *Therm. Sci. Eng. Prog.* **2020**, *18*, 100535.

56. Kumar, T.D.; Hussain, S.S.; Ramesha, D. Effect of a zinc oxide nanoparticle fuel additive on the performance and emission characteristics of a CI engine fuelled with cotton seed biodiesel blends. *Mater. Today Proc.* **2020**. [CrossRef]

57. Habibullah, M.; Masjuki, H.H.; Kalam, M.; Fattah, I.R.; Ashraful, A.; Mobarak, H. Biodiesel production and performance evaluation of coconut, palm and their combined blend with diesel in a single-cylinder diesel engine. *Energy Convers. Manag.* **2014**, *87*, 250–257.

58. Sharma, A.; Murugan, S. Potential for using a tyre pyrolysis oil-biodiesel blend in a diesel engine at different compression ratios. *Energy Convers. Manag.* **2015**, *93*, 289–297.

59. Nanthagopal, K.; Ashok, B.; Tamilarasu, A.; Johny, A.; Mohan, A. Influence on the effect of zinc oxide and titanium dioxide nanoparticles as an additive with Calophyllum inophyllum methyl ester in a CI engine. *Energy Convers. Manag.* **2017**, *146*, 8–19.

60. Karthikeyan, S.; Elango, A.; Prathima, A. Performance and emission study on zinc oxide nano particles addition with pomolion stearin wax biodiesel of CI engine. *J. Sci. Ind. Res.* **2014**, *73*, 187–190.

61. Ramalingam, S.; Chinnaia, P.; Rajendran, S. Influence of compression ratio on the performance and emission characteristics of annona methyl ester operated DI diesel engine. *Adv. Mech. Eng.* **2014**, *6*, 832470.

62. Mohammed, E.K.; Nemit-allah, M.A. Experimental investigations of ignition delay period and performance of a diesel engine operated with Jatropha oil biodiesel. *Alex. Eng. J.* **2013**, *52*, 141–149.

63. Khan, H.; Soudagar, M.E.M.; Kumar, R.H.; Safaei, M.R.; Farooq, M.; Khidmatgar, A.; Banapurmath, N.R.; Farade, R.A.; Abbas, M.M.; Afzal, A.; et al. Effect of Nano-Graphene Oxide and n-Butanol Fuel Additives Blended with Diesel—Nigella sativa Biodiesel Fuel Emulsion on Diesel Engine Characteristics. *Symmetry* **2020**, *12*, 961.

64. Farade, R.A.; Abdul Wahab, N.I.; Mansour, D.-E.A.; Azis, N.B.; bt. Jasni, J.; Soudagar, M.E.M.; Siddappa, V. Development of Graphene Oxide-Based Nonedible Cottonseed Nanofluids for Power Transformers. *Materials* **2020**, *13*, 2569.

65. Mujtaba, M.A.; Masjuki, H.H.; Kalam, M.A.; Ong, H.C.; Gul, M.; Farooq, M.; Soudagar, M.E.M.; Ahmed, W.; Harith, M.H.; Yusoff, M.N.A.M. Ultrasound-assisted process optimization and tribological characteristics of biodiesel from palm-sesame oil via response surface methodology and extreme learning machine-Cuckoo search. *Renew. Energy.* **2020**. [CrossRef]